SEMMELWEIS EGYETEM

DOKTORI ISKOLA

Ph.D. értekezések

2529.

GYÖRGYEY ÁGNES

A vérkeringési rendszer normális és kóros működésének mechanizmusai

című program

Programvezető: Dr. Benyó Zoltán, egyetemi tanár

Konzulens: Dr. Lacza Zsombor, tudományos főmunkatárs

IN VITRO INVESTIGATION OF THE SUITABILITY OF RESTORATIVE AND IMPLANT MATERIALS FOR THE PREVENTION OF DENTAL IMPLANT ASSOCIATED INFECTIONS

Ph.D. Thesis

Ágnes Györgyey

Semmelweis University

PhD School of Basic and Translational Medicine

Consultant: Zsombor Lacza, MD, DSc
Official Reviewers: Rita Kiss, Dsc
Árpád Joób-Fancsaly, DDS, PhD

Head of the Complex Examination Committee:
Barna Vásárhelyi, MD, DSc,

Members of the Complex Examination Committee:
Péter Andréka, MD, PhD
Ákos Zsembery, MD, PhD

Budapest

2020

TABLE OF CONTENTS

1 LIST OF ABBREVIATIONS

AB	AlamarBlue®
AFM	Atomic force microscopy
AgNP	Silver Nanoparticles
ALP	Alkaline Phosphatase
ANOVA	One-way Analysis of Variance
BIC	Bone to Implant Contact
BHI	Brain Heart Infusion
BOP	Bleeding on Probing
CA	Contact Angle
CoCr	Cobalt Chromium
ECM	Extracellular Matrix
EDTA	Ethylenediaminetetraacetic acid
EMEM	Eagle's Minimal Essential Medium
FBS	Fetal Bovine Serum
FWHM	Full Width at Half Maximum
KrF	Krypton Fluoride
MALDI-TOF MS	Matrix-assisted Laser Desorption/Ionization Time-of-flight Mass Spectrometer
MSC	Mesenchymal Stem Cell
MEM-α	Alpha Modification of Eagle's Medium
MTT	3-(4,5-dimethylthiazol-2-yl)-2,5-diphenyltetrazolium bromide
Nd:YAG	Neodymium-doped Yttrium Aluminum Garnet
NP	Nanoparticle
OD	Optical Density
PBS	Phosphate Buffer Saline
p(EA-co-MMA)	Poly(ethyl acrylate-co-methyl methacrylate)
PMMA	Poly-methyl-methacrylate
Ra	Average Roughness
RT	Room Temperature
SEM	Scanning Electron Microscopy
SLA	Sand-blasted, Large grit, Acid etched
Ti	Titanium
TiO_2NP	Titanium Dioxide Nanoparticle
UVC	Ultraviolet C
UV-VIS	Ultraviolet–Visible
XPS	X-ray Photoelectron Spectroscopy

2 INTRODUCTION

Peri-implant infection (peri-implantitis) has become the leading cause of the failure of dental implants. Epidemiological data vary in a wide-range in the literature concerning the prevalence and incidence of peri-implantitis presumably for two reasons. One reason might be the unclear definition of the medical condition in terms of diagnostic parameters. Data in the literature show that there are dentists who diagnose milder medical pictures as peri-implantitis than others. The other reason might be the uncertainty that is often associated with the aetiology of the peri-implant infections. In some cases, bacterial events without unknown causatives are in the background (primary peri-implantitis), while the pathological loading of the implant due to inappropriate implantation and/or prosthetic treatment may end up in the same clinical picture (secondary peri-implantitis). The currently available therapeutic options are not effective in the treatment of peri-implantitis, the progression of the biofilm formation might only be slowed down, but the infected implant will be lost in the end. Hence, the prevention of the peri-implantitis is regarded as a more effective management option than the treatment. To this end, the enhancement of the biological performance of dental implants has been in the focus in the last few decades both in the industrial and academic researches. Since the geometry of the dental implants has by and large consolidated, the research and development activities shifted towards the improvement of the implant surfaces. One strategic approach has been the improvement of the biocompatibility of dental implants ensuring complete biological sealing around the implant in order to exclude pathogenic bacteria from the implant site. A more recent approach is the enhancement of the antibacterial feature of the surface of dental implants with the view to create an 'active' line of defence against bacterial infections (Figure 1).

In my doctoral work I attempted to appraise and put into context the current research and development trends that are related to the prevention of the peri-implant infections of dental implants. In this endeavour I performed *in vitro* studies in this domain to verify untested hypotheses relating to the biological sealing of prosthetic materials, investigated the suitability of innovative laser ablation methods for the improvement of the biocompatibility of medical grade titanium, and examined the antibacterial attribution

of a novel coating nanocomposite. The clinical management, i.e. treatment of peri-implantitis is beyond the scope of the present doctoral work.

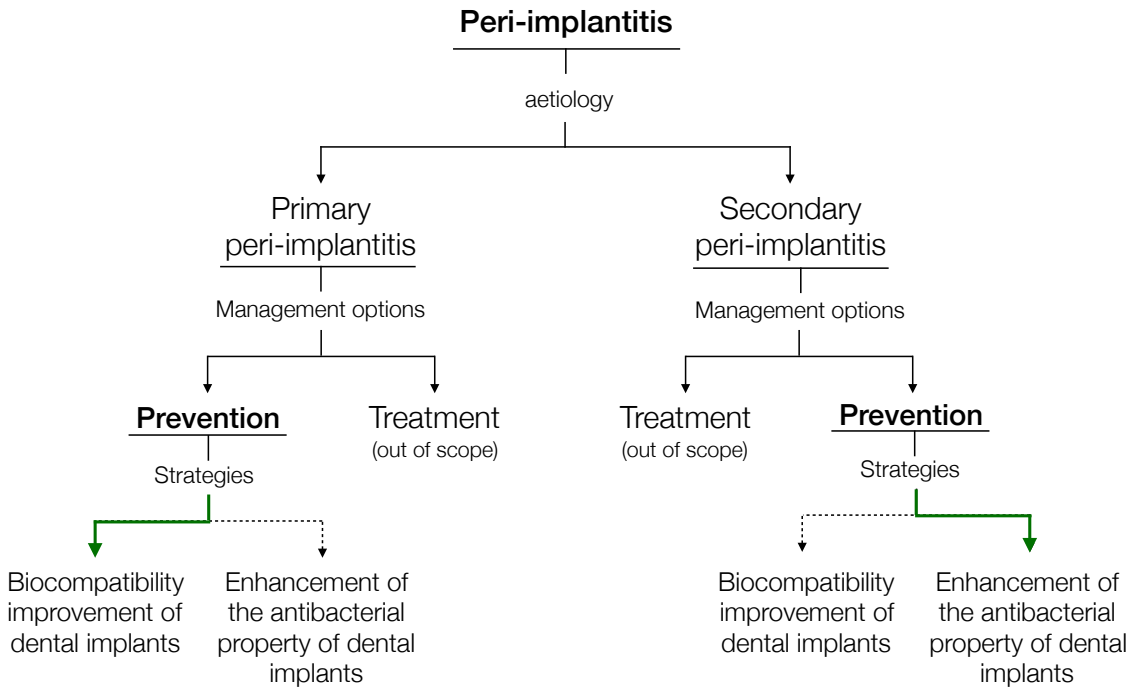

Figure 1 shows the schema of the present doctoral work. The causatives of peri-implantitis can be related to bacterial (primary peri-implantitis) and non-bacterial events (secondary peri-implantitis) that should be taken into consideration in the development of strategies for the prevention. Secondary peri-implantitis might be the consequence of inappropriate implant placement and/or prosthetic work that trigger constant local inflammation at the implant site. To reduce the risk of the development of secondary peri-implantitis in the inflamed tissue the enhancement of the antibacterial property of dental implants could be a reasonable strategy. In contrast, when complications associated with implantation and prosthetic work can be excluded then the risk of primary peri-implantitis could be reduced by the improvement of the biocompatibility with the view to support gap-free closure around the implant. Green lines indicate the preferred prevention approaches in the binomial decision tree, dotted lines and arrows indicate supplementary solutions. The structure of the present doctoral work follows this schema, and its objectives were set accordingly. Source: own construction.

2.1 Dental implants

Dental implants are medical devices that are intended for the replacement of missing teeth. They are surgically inserted screws into the maxillary or mandibular bone. After a

successful healing and integration period the intraoral parts of prosthetic restorations, such as crowns, bridges or removable dentures are held by indwelling screw implants that also bare and transmit the forces of mastication to the surrounding bone. Nowadays, dental implants are the first choice of dentists to replace missing teeth because they offer the best option to restore the original aesthetic and function of the lost teeth compared to alternative prosthetic solutions. In some cases, implant-based restored dentition can give the patient the sensation of having their own teeth back. Yet, no other prosthetic solution has this advantage (1, 2). Figure 2 shows the schematic presentation of an implant retained crown.

The integration of a dental implant into the jawbone (osseointegration) is strongly influenced by its macrostructure, such as size, geometry and the curves of the implant as well as the angle of the thread, and the sizes of the thread in metric scale of millimetre to micrometre (3-5). In the past few decades the geometry of dental implants has more or less been consolidated and the focus of research and development activities has shifted towards the improvement of surface properties (6). The surface topography has been considered pivotal to ensure the short-, and long-term stability of dental implants in the jawbone. To this end, a wide-range of rough surfaces have been developed using various surface treatment techniques and technologies (7). More recently, particular attention has been payed to nano-topographies (0-100 nm) (8).

Figure 2 shows the three primary parts of a dental implant. The implant body (4) is placed into the jawbone providing a permanent foundation. Abutment (3) and screw (2) support the permanent connection between the implant body and crown. Implant crown (1) is the part that looks like a natural tooth, it gets either screwed or cemented to the abutment. Figure and legend are reprinted from reference (9).

2.2 Dental implant materials

The material of dental implant must be biocompatible and be able to transmit the mastication forces to the jaw. The long-term success of dental implant-based restorations depend primarily on four factors: i) the quality of osseointegration of the implant; ii) the peri-implant mucosal seal i.e., the protection of the implant from bacterial infections from the oral cavity; iii) the adequate transmission of the mastication forces to the implant body from the abutment and iv) the mechanical properties of the material of the implant (10-13). At the current level of technology titanium and zirconia (zirconium-oxide) are regarded suitable to fulfil these requirements (14).

2.2.1 Zirconia dental implants

Zirconia is mostly chosen for its aesthetic appearance because it mimics the colour of natural teeth. Zirconia occurs in three crystal structures: monoclinic, tetragonal and cubic. Monoclinic form is stable at room temperature (RT) up to 1170ºC, what involves the circumstances found in human bone and the oral cavity. Since its tetragonal form, that is stable at 1170–2370°C, has much more favourable properties for implant applications, such as high flexural strength, superior corrosion and wear resistance, efforts are made by manufacturers to keep zirconia in this state in the oral circumstances, i.e. at lower temperature. This can be achieved by adding stabilizing oxides, such as CaO, MgO, Y_2O_3, or CeO_2. Still, surface modification of the zirconia implants, and contact with moisture in the bone or the oral cavity contribute to a tetragonal to monoclinic transformation that is associated with volume expansion resulting in the formation of cracks. Until this transformation is slow and slight the volume expansion results in the compression of the cracks, but when its rate increases it weakens the material and leads to aging resulting in fatigue fracture (15). In addition, volume changes result in deformities in the shape of the implant and in the fitting of the connecting abutment allowing micromovements that is supposed to be a causative of the failure of implants in the long run (see chapters below).

Another difficulty in conjunction with zirconia implant design is the brittle nature of ceramics, meaning that stress concentration on any points and surfaces should be avoided otherwise the ceramic material breaks. Sharp, deep threads, internal joining surfaces can act as stress points, however, these are necessary macrostructural characteristics of a *lege artis* dental implant (16). Survival of zirconia-based restorations is already well documented. Failure due to aging occurs mostly in two years regardless of the type of restoration (17, 18). Nevertheless, the survival of zirconia implants is yet very poorly documented. Some studies showed only one-year survival of the zirconia implants even though the first year is eventless, usually (19, 20). Clinical data on the 5-years survival of zirconia implants should be available to credibly prove their performance but only a few follow-up studies can be found. There is a strong interest in finding a metal-free, aesthetic solution to implant-based rehabilitation, but the durability of zirconia is yet not comparable to that of titanium.

Owing to their poor mechanical properties the share of zirconia implants is only a fraction of the total market which is dominated by titanium implants. Thus, the focus of my doctoral work was limited to titanium dental implants.

2.2.2 Titanium dental implants

The vast majority of the available implants on the market is made of titanium because it has a relatively lower mechanical mismatch with the bone compared to zirconia and other metals/alloys, while exhibits excellent biocompatibility with human tissues (21). Concerning implant applications, six so-called medical grade titanium implant materials are in use, i.e. grade 1-4 that are commercially pure, grade 5 is an alloy of titanium with 6% aluminium and 4% vanadium (also known as Ti6Al4V) and grade 23 (also known as Ti6Al4V ELI), which is considered a higher purity grade than grade 5 due to the lower inclusions of iron. The mechanical characteristics, such as tensile strength, flexibility stems from the bulk properties of titanium. There are significant differences, for example, in the tensile strength of the various grades, which ranges from 240 to 550 MPa concerning grade 1-4, 895-930 MPa for grade 5 and 860-965 MPa for grade 23 (22). The indwelling part of an implant that is placed into the bone tissue (also known as fixture or implant body) is made of grade 2 or grade 4 titanium in most of the cases, while abutments and screws are made of grade 5 or grade 23, usually.

When metallic titanium is exposed to air or water an oxide layer develops on its surface. This oxide layer provides good resistance to corrosion and facilitates the osseointegration (23). A gradient of the oxidation states of titanium can be observed in the titanium-oxide layer: $TiO \rightarrow Ti_2O_3 \rightarrow TiO_2$. The most stable oxide of titanium is TiO_2, which constitutes the outer oxide layer and responsible for the biocompatibility and the osseointegration of titanium implants (23).

2.3 Improvement of the biocompatibility of dental implants

2.3.1 Biocompatibility: overview and definitions

When a foreign material is placed into the human body its fate depends on the host response. The ability of a foreign material for the replacement of body parts or tissues is described by the term 'biocompatibility'. Biocompatibility is often used in the literature; however more specific terms may be useful to describe and understand the biological behaviour of the various materials in particular indications. Biocompatible materials that are intended for tooth replacement can be divided further into subcategories, like biotolerant, bioinert and bioactive materials (24). Biotolerant materials, upon being placed into the bone tissue are separated from the bone tissue by a layer of fibrous tissue. If fibrous tissue develops around the implant, the surrounding bone tissue keeps its ability to recover, however direct bone-material contact will not develop. Typical examples for biotolerant materials are poly-methyl-methacrylate and stainless steel (25, 26). Bioinert materials facilitates the development of direct bone-material interaction, however some fibrous tissue formation may still happen. Examples for bioinert materials include titanium alloys and zirconia (27). Bioinert and biotolerant materials make physical bond with the bone tissue. In contrast, bioactive materials chemically and/or biologically interact with the surrounding bone tissue. Briefly, ion exchange reaction occurs between the bioactive material and surrounding body fluids resulting in the formation of a biologically active apatite layer on the surface of the material, which is chemically and crystallographically equivalent to the mineral phase of the bone (28). Examples of bioactive materials are synthetic hydroxyapatite and glass ceramics/bioglasses (29, 30).

2.3.2 Osseointegration of dental implants: a clinical perspective

When an implant surgery takes place the healing process can be defined from a clinical point of view. Before the insertion of the implant a cylindrical hole is predrilled into the jawbone. The surgeon must decide on the size of the predrilled hole by taking into consideration the diameter of the implant. The diameter of the prepared hole can have

the size of the outer threads of the inserted implant (i), the size of its inner threads (ii) or in between (iii). The size of the hole affects the bone healing. In the first case (i), when the hole has the size of the outer thread, the body of the implant has the largest distance to the bone. The insertion of the implant does not make any extra stress or injury to the bone and so-called healing chamber forms where undisturbed healing can begin. This solution gives less primary stability to the implant, but it is supposed to enhance the secondary stability later on. Primary stability can be defined as the mechanical anchorage of the implant to the bone right after the implant surgery. Secondary stability can be described as the biological fixation of the implant in the bone after its complete osseointegration (31). In the second case (ii), microcracks appear in the bone during the insertion of the implant and compression necrosis can also be observed later on. In this case, high primary stability can be achieved, though it declines after some weeks due to the mechanical stress induced necrosis of the surrounding bone tissue. In the third case (iii), both structures can be observed; healing chamber appears accompanied with slight necrosis (32). The understanding of these physiological processes has been important to decide on the appropriate prosthetic treatment and on the loadability of the implant.

The first week of undisturbed healing is critical for the proper osseointegration of a dental implant, however it is compromised by the invasive nature of the implant surgery. The first step of an implant surgery is the creation of a surgical flap when gingiva is incised and separated from the bone. At this point, prior to drilling the hole for the implant the sterile, intact bone gets into contact with the bacterial flora of the saliva. After the surgery and the closure of the gingival flap it takes one week for gingiva of a healthy patient to close completely over the implant site. Owing to the incomplete biological sealing the protection of the wound is extremely important in this early period because bacteria can easily penetrate the implant site. When the healing process is undisturbed the osseointegration is observed by the 6th week, usually. The drilled hole is filled with neoformed, immature bone, though some empty lacunae can still be found (33). Neoformed bone has a woven, irregular microarchitecture that resulted from rapid growth (12).

Lamellar bone formation and remodelling start during the 7th-12th week. This process begins already without the loading of the bone. Later, when the mature bone is

loaded these lamellae are aligned with the mastication forces that are transferred by the osseointegrated implants to the jawbone. Tractive or squeezing forces always rearrange lamellae in alive bone (34). The secondary stability of an implant largely depends on the bone formation around the implant and on the remodelling phase. According to Wolff's law, the subsequent phase of load oriented bone remodelling leads to a replacement of primary woven bone to realigned lamellar bone in order to optimize the absorption of occlusal loading and to transmit the mechanical stimuli to the adjacent bone tissue (32).

2.3.2.1 Primary and secondary stability of dental implants

The increasing demand of patients to complete the implant surgery and prosthetic work in one sitting has put pressure on dentists to offer treatments that allow the immediate loading of implants; however, at the current level of technology, long-term risks might be associated with such interventions. Primary stability is regarded as the paramount diagnostic parameter to make decision on the feasibility of the immediate loading of implants. The primary stability of an indwelling dental implant is measured by resonance frequency analysis and is quantified on Implant Stability Quotient (ISQ) scale ranging from 1 to 100 (35). Empirical evidence suggest that ISQ score above 70 stands for high primary stability, while ISQ score below 60 stands for low primary stability. According to recent papers an implant may only be loaded immediately if its ISQ score is above 65; though, there is no official guideline that supports the empirical data with objective evidence (36). In fact, the available scientific evidence do not support that the ISQ score is a suitable measure to predict the long-term survival of the implant. The primary stability is not a constant parameter, it decreases in time after the implant placement because of the resorption of the surrounding bone tissue, but in the meantime the simultaneously growing new bone tissue is insufficient to provide proper secondary stability to the indwelling implant. Owing to these concomitant processes of initial bone remodelling the stability of the dental implants decreases after the implantation reaching a minimum between the 2nd and 3rd weeks (Figure 3) (37).

According to Rodrigo and his colleagues there is no correlation between implant survival and primary stability, but there is between secondary stability that is measured

after the healing period right before the prosthetic work (38). Other authors also stated that there is no link between the primary and secondary stability of implants even if the healing period was eventless (39, 40). The result of my literature search coincides with these opinions, it did not reveal any paper that prove the correlation between primary stability and implant survival, either. Nonetheless, other authors state that primary stability is routinely used as a diagnostic parameter to predict the outcome of the implant surgery, however the available evidence do not support its suitability, especially when it comes to immediate loading (36, 37).

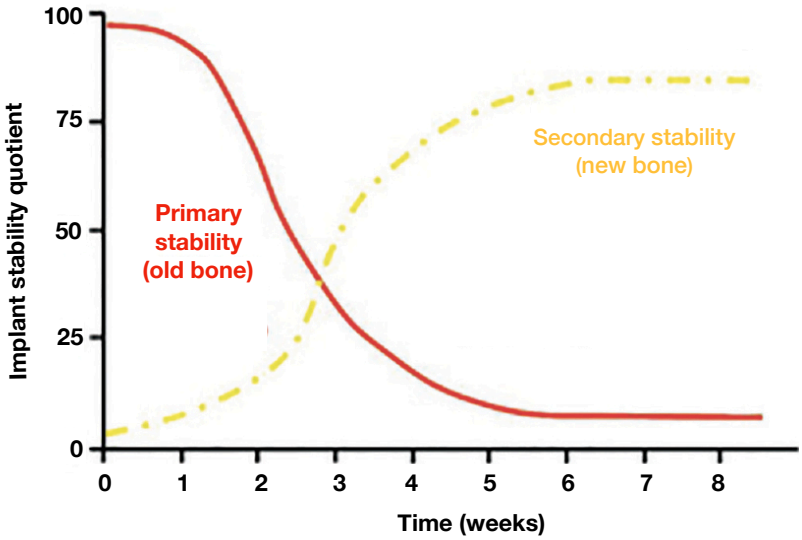

Figure 3 shows the kinetics of change in primary and secondary stability of dental implants. The primary stability of the implant decreases in time owing to bone remodelling reaching the minimum approximately at the 3rd week. Secondary stability comes with the mineralization of the newly formed bone tissue leaving a 'vulnerable' period in terms of loadability of the implant in the course of osseointegration. Figure is reprinted from reference (37).

2.3.2.2 Critics of universal dental implants

The properties of the bone are to be taken into account in the course of the planning of implant surgery. Various categorizations have been published based on the characteristics and suitability of trabecular and cortical bone for implantation. Typically, microscopic and tactile investigations constitute the basis of categorizations. However, there are systems that consider the proportion of the cortical and trabecular bone, others compare the hardness of the bone to that of wood, while clinical experience-based empirical categorizations also exist (41). The disadvantage of all these systems is that they cannot support the upfront planning of the implant surgery, the underlying characteristics of the bone can only be experienced during the invasive surgery. Cone Beam CT is regarded as a suitable and widely-used mean to evaluate the bone quality prior to the implant surgery. The processing of captured CT images allows the measurement of bone density in Hounsfield units. Misch suggested the categorization of the various bone structures based on density (Table 1) (42). The weakness of this categorization lies in the diversity of image processing of the various imaging systems that may lead to inaccurate results, though it is widely used in the clinical practice (43). However, in order to maximize the clinical outcome and so the benefit to the patient, that is, the long-term survival of dental implants, it would be critical to choose the appropriate type of the implant by taking into consideration of the available bone structure (quality) and the applicable (matching) prosthetic abutments that can suitably transfer the mastication forces to the jaw bone. In addition, the geometry of the implant, the angle, density and edge of the thread significantly influence the forces and tensions that are generated in the bone during the implant placement and also play important role in the transmission of the mastication forces to the surrounding bone tissue, and so influence the long-term survival of the implant (44-46).

The design of the current implants does not allow differential treatment of the patients; thus, they are universally used in various clinical pictures. There are some implant brands that may provide incremental benefit to the patient in particular situations, but in most of the cases these options are abandoned. The price of the implant has been a more important parameter than the benefit-risk profile of the applied surgical technique

or implant type. Hence, clinics usually have one or two implant systems, whose primary distinctive characteristic is the price, but not the functionality. This is because the installation cost of a new implant system is high and the learning curve, the time period until the surgeon gets familiar with the new system, takes few years reducing revenues due to low relative effectiveness. In order to avoid this loss of income, the dentists are unwilling to invest into a broad-range of implant systems because of the anticipated long pay-back period.

Table 1 shows the categorization of bone structures based on bone density. The higher value refers to higher bone density. Source: own construction based on reference (42).

Bone structures	Hounsfield unit
D1	> 1250
D2	850 – 1250
D3	350 – 850
D4	150 – 350
D5	< 150

2.3.3 Surface modification of titanium dental implants

2.3.3.1 Purpose of surface modifications

When bone substitutes are placed into the human body, interactions between their surface and the surrounding bone and soft tissues are critical to osseointegration. Surface topography of bone substitutes is supposed to influence bone response and plays a major role in both the quality and rate of osseointegration. Micro-rough TiO_2 surfaces, such as sandblasted/acid etched (SLA) surfaces have long been suggested to be optimal to support the osseointegration of dental implants (6, 21, 47, 48). Wennerberg and Albrektsson divided surfaces into four groups according to their surface roughness at micrometre level (Table 2).

There is an increasing demand from the patient's side for a shorter healing time and a quicker rehabilitation. Normally, the implants are not loaded for three months after

the insertion until the osseointegration is completed, and the prosthetic rehabilitation is mostly done subsequently. During this period, patients must wear temporary prostheses which allow limited eating, speaking and social functions. This explains the need and effort to accelerate osseointegration.

Many approaches can be found in research papers to solve the problem of long healing time or disturbed osseointegration. One trend is to improve the biocompatibility of the surface of the implant and so to speed up the osseointegration process. This can be achieved by topography improving techniques or by surface coatings. Another scientific approach is to improve the bacterial resistance of the surface, and so to create a surface that can resist the bacteria of the oral flora, when the healing is disturbed or when post-osseointegration peri-implant infections occur. To this end, antibiofouling titanium surfaces and antibacterial coatings have been developed (Figure 4).

Table 2 shows the arbitrary categorization of micro-rough surfaces. Sa (arithmetical mean height) expresses, as an absolute value, the difference in height of each point compared to the arithmetical mean of the surface. This parameter is used generally to evaluate surface roughness (49).

Micro-rough surfaces	Sa
Smooth surface	Sa: <0,5µm
Minimally rough surface	Sa: 0,5-1 µm
Moderately rough surface	Sa: 1-2 µm
Rough surface	Sa: >2 µm

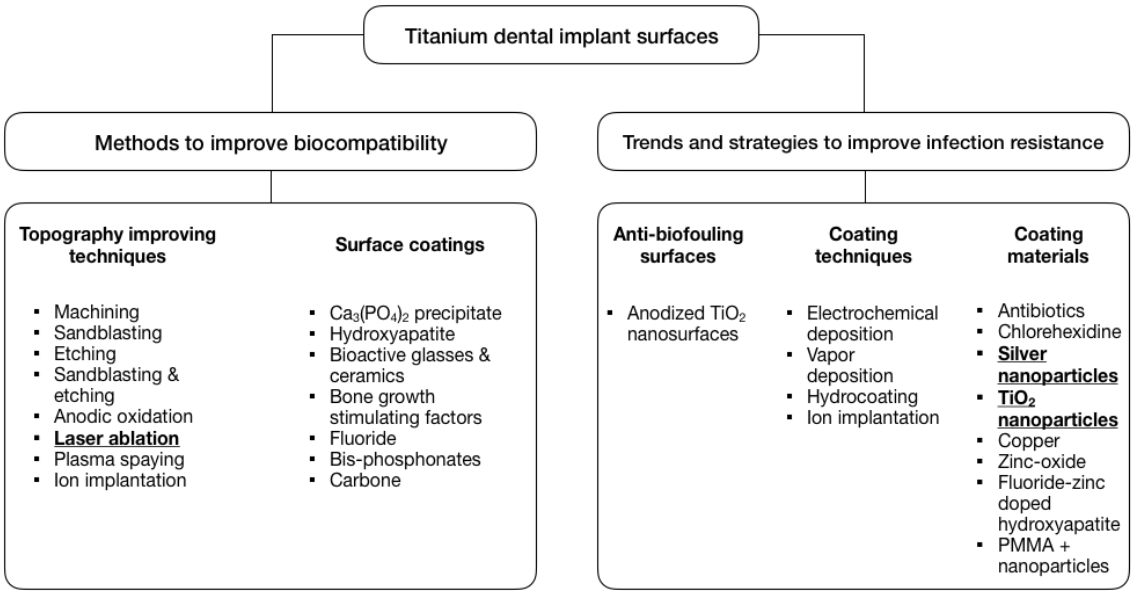

Figure 4 shows the current trends in surface modification of titanium dental implants. The research and development activities can be divided into two branches. One is the improvement of the biocompatibility, while the other is the enhancement of the bacterial resistance. The methods that are used for the improvement of the biocompatibility can be categorised as topography improving and coating techniques. Topography improving relies on the manipulation of the TiO_2 layer on the surface of dental implants, while coating techniques are intended to adhere other substances to the TiO_2 layer. Concerning antibacterial surfaces, in fact, the same categorization applies, that is, topography improving to grow TiO_2 nanosurfaces on dental implants (for instance, antibiofouling surfaces), and coating by using chemical substances or materials of antibacterial property. There is a large diversity in the applied coating and topography improving techniques, including physical, chemical and physicochemical methods. The bold, underlined techniques and materials are further discussed in the experimental parts of the present doctoral thesis. Source: own construction.

2.3.3.2 Dental implant surface types in clinical use

Sandblasted plus acid etched (SLA) surfaces are the most often applied on titanium dental implants. The SLA treatment increases the overall surface area by creating uneven surface features, which is also referred as microroughness in the literature. The SLA surfaces has often been used as 'gold-standard' control in pre-clinical and clinical studies in comparison to novel surfaces because of their predictable *in vitro* and *in vivo* performance. For the time being, no other surface has been proved to be credibly superior to SLA either in pre-clinical or in clinical experimental settings.

The summary of dental implant surface types that a large population is exposed with, and the associated product brands along with the manufacturers are shown in Table 3. In principle, the clinical performance and safety of dental implants is supposed to be justified in a sequence of mechanical, pre-clinical and clinical studies, especially when surface treatment is applied in order to modify the biological characteristics (50). There are relevant standards for the *in vitro* characterization of dental implants, albeit the vast majority of the published studies have been carried out according to different protocols making unreliable the comparison of the biological characteristics of the various surfaces. Even larger diversity can be observed in the experimental protocols of clinical studies with dental implants, however the quantity of published randomised controlled clinical studies is extremely low compared to the number of commercialised implant brands (51). Based on the results of a systematic literature review the summary of the pre-clinical and clinical advantages and disadvantages of the commercially available surfaces are shown in Table 4. Apparently, the results are often contradictory, it is not possible to extrapolate to the *in vivo* performance based on *in vitro* results and vice and versa. Hence, the evaluation of the available data is intuitive rather than evidence-based concerning the comparative clinical advantages of the various implant surfaces.

Dental implant manufacturers produce commodity products that are intended for universal application, that is, the replacement of missing teeth. This product policy is in line with the business interest of the manufacturers however ignores the variety of possible clinical pictures, including but not limited to the transmission of mastication forces from the crown and abutment to the indwelling implant body. Clinical studies have been designed according to this universal approach, i.e. the success rate of the implants is measured under various load in most of the cases. This is why it is not possible to gather relevant information about the different properties of the dental implants. For instance, it does not make any sense to compare two implants with different surfaces, if the type of the cutting edge of the threads are different, too. The fine-tuning of the surface characteristics may add value to clinical performance of an implant that could be utilized in the management of some particular clinical situations. However, the current experimental design of the clinical studies is not sensitive enough to detect such fine differences in the clinical performance of dental implants. At the current level of

technology, it is not supposed to be the challenge to prove the success rate of implants in selected groups of patients, but to provide solution for unconventional cases ensuring implant survival beyond 5 years.

Table 3 shows the surfaces of commercially available dental implant brands. Source: own construction.

Brand/surface type	Surface modification	Manufacturer
SLA	Sandblasted/large grit/acid etched (SLA)	Straumann, Camlog, DIO, Ankylos, SGS
Straumann SLActive	SLA in 0,9% NaCl solution under N_2 atmosphere	Straumann
CA	Activated SLA in Ca^{2+} solution	Osstem
MP-1 HA	Grit blasting with HA, pressurized, hydrothermal, post–plasma spray process	Zimmer
BCP	Grit blasting with HA and β-TCP	Anthogyr
OsseoSpeed	Grit blasting with added fluoride (etched with HF) (5)	Astra Tech
TiUnite	Spark anodization with phosphoric acid	Nobel Biocare
Xpeed	$CaTiO_3$	Megagen
Ossean	SLA and CaP impregnation (robotic microblasting with resorbable media powder) (5)	Intra Lock
NanoTite	CaP discrete crystalline deposition (DCD)	3i
Laser Lok	Laser machined cell sized channels on the collar of the implant	Bio Horizons

Table 4 shows the advantages and disadvantages of various implant brands based on available pre-clinical and clinical data. Source: own construction.

Surface name	Preclinical advantage	Preclinical disadvantage	Clinical advantage	Clinical disadvantage
SLA	▪ Affordable manufacturing process ▪ Large increase of surface area is achievable ▪ Superior or equivalent *in vitro* performance compared to other surfaces (52)	▪ Increased bacterial attachment compared to polished surfaces (53)	▪ Good clinical results (54) ▪ Clinical evidence was not found of a correlation between SLA surface and peri-implantitis (55) ▪ No other surface was proved superior in a >5 years interval	▪ Unknown (current gold-standard)
Straumann SLActive	▪ Bioactive (according to ISO 23317) (56) ▪ Increases in ALP, osteocalcin (57, 58), prostaglandin E2, TGF-β levels (59-61)	▪ Similar cell attachment compared to SLA (62, 63) ▪ No differences in buccal bone level and BIC in beagle dog study after immediate implantation compared to NanoTite and TiUnite (64)	▪ Stronger short term response compared to SLA (54) ▪ Increased implant stability during healing (65)	▪ Unknown compared to SLA: ▪ Differences disappear after the first 6-8 weeks ▪ No reported difference in bone loss (54)
CA	▪ Histologic proof of early osseo-integration in sheep model (66)	▪ *In vivo* results are not detectable with RFA or radiographic analysis (3, 66)	▪ No data found	▪ No data found
MP-1 HA	▪ Mechanically stable coating (4, 67) ▪ Decreased *in vitro* solubility (68)	▪ pressurized hydrothermal post-plasma-spray process resulting in higher HA levels does not affect the osseointegration rate *in vivo* (67)	▪ Only one clinical study on the 5-years long survival showing cumulative implant success of 97% (69)	▪ No data found
BCP	▪ Increased surface roughness (70)	▪ No significant *in vitro* adhesion, proliferation or differentiation differences compared to SLA (71)	▪ No data found	▪ No data found
Osseospeed	▪ Facilitates osteoblast differentiation and mineralization (72) ▪ Stronger cell-attachment compared to machined surface (73) ▪ Enhanced osteogenic gene expression suggesting osteoinductive properties (74, 75)	▪ Not bioactive (56) ▪ No differences in viability or proliferation compared to sandblasted surface (72)	▪ Increased bone-implant contact compared to sandblasted surface (76)	▪ No available data in comparison with other commercially available implants
	▪ Enhanced adhesion, proliferation and differentiation (77)	▪ Little is known about the mechanical resistance of the layer (78) ▪ Not bioactive (56) ▪ No differences in buccal bone level and BIC in beagle dog study after immediate implantation compared to SLActive and NanoTite (64)	▪ Long-term results of reduced failure and clinical reliability compared to turned surface (79)	▪ Superiority to (bone level, survival) turned implants is not proven (37, 79) ▪ No significant differences in long-term marginal bone level in meta-analysis (80)

Continuation of Table 4

Surface name	Preclinical advantage	Preclinical disadvantage	Clinical advantage	Clinical disadvantage
Xpeed	▪ Increased osteoblast adhesion compared to untreated titanium (81) ▪ Increased bone to implant contact and removal torque *in vivo* (82)	▪ Higher *in vitro* attachment of A. actynomicetemcomitans and P. gingivalis (83)	▪ No comparable data	▪ No statistical differences when compared to other resorbable blasted media surfaces (84)
Ossean	▪ Enhanced bone mineralization after 1 and 2 weeks in *in vivo* rat study (85) ▪ Significantly lower buccal bone loss in canine study (86) ▪ Increased torque removal in dog model compared to dual etched surface (87)	▪ No significant differences in gene expression at 4- and 8-week time points in rat study compared to dual acid-etched surface (85) ▪ non-significant differences in BIC% in canine model compared to dual etched surface (87)	▪ No data found	▪ No data found
NanoTite	▪ Promising *in vivo* results in rodent models compared to TiOblast (only sandblasted) surface (88, 89)	▪ Significantly lower cell confluence compared to Osseospeed and Straumann SLA (90) ▪ Inferior results in primary mouse alveolar bone cell culture model compared to Osseospeed (90) ▪ No differences in bone response in rabbit model compared to SLA (91) ▪ No differences in buccal bone level and BIC in beagle dog study after immediate implantation compared to SLActive and TiUnite (64)	▪ High success rate in 1-year clinical study (92)	▪ No data found ▪ Studies available on immediate loading but without reference to control surface (92)(NCT00713206)
Laser Lok	▪ In mongrel dog study higher BIC after 12 weeks compared to turned surface (93) ▪ Diminished loading stress at collar part in FEA evaluation investigating bone attachment (94)	▪ After 3 months of healing and 6 months of loading, no differences were detectable in bone height (95)	▪ Connective tissue attachment to the collar (96) ▪ Clinically reliable for immediate implantation (within 2 years) (97) ▪ Good clinical results after immediate loading with fix restorations (98) ▪ Stable soft tissue seal and smaller crestal bone loss at 37 months compared to other implant with machined control (99)	▪ No data found, ▪ Case study with a limited number of implants involved (100)

2.3.3.3 Lasers in surface modifications

Lasers offered a relatively new and promising alternative of the current surface treatment methods because of their precision and rapidness. They also allow the custom-made preparation of the surface in the various regions of the implant providing comparative clinical advantage against uniform surface patterns (101, 102).

Various lasers are used for titanium surface modification, like CO_2, Nd:YAG, excimer, dye, argon-ion and diode lasers [35]. The mode of action of lasers in surface modification is the melting and evaporation of the material that absorbs laser beam. Concerning Nd:YAG laser, prior to ablation of a material, the absorption of radiation raises temperature of the surface resulting in its melting. As the temperature continues to rise, vaporization of the material occurs, and finally, it solidifies when the temperature cools down. Melting, melt motion, evaporation, and solidification are the series of steps involved in the generation of new surface topography when a focused laser beam interacts with a material surface (102).

Excimer lasers enable micromachining which is especially useful when the geometry is complex. During ablation, the surface of the material absorbs the radiation leading to a rapid rise in its surface temperature followed by evaporation. Applying high laser intensity in repeated exposures of a same surface area laser texturing/patterning can be achieved [35] (102).

2.4 Microbiological aspects of surface modifications

Nowadays, dental implants are widely used for the replacement of teeth because the achievable benefits for the patients outweigh the associated risks under normal conditions. Nevertheless, disturbed osseointegration, peri-implant infections, placement of implants into at-risk patient populations, the use of low-quality implants and inadequate surgical techniques may detrimentally affect the clinical outcome of the implant surgery. This chapter focuses on peri-implant infections, hence the state-of-the-art is introduced from this perspective in the followings.

2.4.1 Biofilm formation on implants

The sequence of microbial colonization on dental implants and biofilm formation is similar to that of teeth. Species that colonize dental implants are the same that are found in healthy gingiva and in gingivitis sites around teeth (103, 104). Colonizing bacteria are part of the normal flora found in the oral cavity. Fürst *et al.* found that bacterial colonization occurred within 30 minutes after implant placement and early colonization patterns slightly differed between implant and tooth surfaces in the colonizing bacterial species. Periodontal infections and peri-implant infections do not really differ in terms of the composition of the bacterial strains but more in the proportion of these bacteria.

The first step of biofilm formation is the reversible adhesion of early colonizer bacteria mediated by electrostatic and hydrophobic forces. The second step is irreversible adhesion caused by a time-dependent shift to a higher binding affinity state, which involves multiple adhesins on the bacterial surface and polymer matrix. Division of the attached bacterial cells creates microcolonies that further expand until the layer of bacteria becomes confluent. Confluent growth results in the formation of plaque biofilm, which develops in terms of complexity in time (104). The sequence of microbial colonization on dental implants and biofilm formation is similar to that of teeth. A large proportion of the early colonizers are streptococci, such as *Streptococcus sanguis*, *Streptococcus oralis*, *Streptococcus mitis*, found in dental plaque and in the gingival sulcus, and also *Streptococcus salivarius* that is found in the saliva. Actinomyces species may also appear in the earliest stages of biofilm formation. The early colonizers, like streptococci and actinomyces species, create favourable conditions for late colonizers that require a particular environment (104). The early colonizers promote the adhesion of late (often called as secondary) colonizers by co-adhesion. Late colonizers include, for example, *Porphyromonas gingivalis*, *Prevotella forsythia*, *Fusobacterium nucleatum*, *Treponema denticola*, *Streptococcus micros* or *Tannerella forsythia* (105). By the multiplication of early and late colonizer bacteria and the excretion of their self-produced extracellular polymeric matrix biofilm proceeds along the surface of infected implants (103, 104). Subramani *et al.* defined biofilm as a microbial-derived sessile community characterized by cells that are irreversibly attached to a substratum or interface to each other, embedded in a matrix of extracellular polymeric substances produced by microbes

(104). Surface characteristics, such as roughness and surface free energy are supposed to play key roles in biofilm formation (104). The most bacterial attachment was observed on rough titanium surfaces, whereas on smooth surfaces they showed poor attachment (103). Titanium samples that exhibited rough or hydrophobic surfaces showed higher degrees of bacterial colonization (106).

2.4.2 Disturbed osseointegration and wound healing

In the course of the placement of the implant the exposure of the wound to bacterial contamination can be minimalized if the surgery is performed in compliance with the sterility and other applicable guidelines (107). Nevertheless, in the subsequent week of the implantation, until the full closure of the protective epithelium barrier around the implant the wound may get infected from the oral cavity (108). If infection occurs, the healing of the implantation site is disturbed, which may prolong the process or even end up in the failure of the implant (109) (110). Hence, the compliance of the patient for at least one week after the implantation is critical for the survival of the implant. In contrast, there are multiple lifestyle related factors that increase the probability of the infections, such as inappropriate oral hygiene, smoking, and alcoholism (110, 111). The general health status of the patient, comorbidities and concomitant treatments may also detrimentally affect the clinical outcome of implant surgery, for example, diabetes, steroid therapy, chemotherapy and radiotherapy (111). In addition, iatrogenic factors, like poor planning and surgical technique, for example, weak sutures, bad flapping also increase the risk of infections (112).

If the surgical site gets infected and it is not recognized in a timely manner the invasion of bacteria will reach the surface of the implant causing a non-sterile inflammation in the surrounding bone and soft tissues (113). In the course of non-sterile inflammation fibroblast are recruited at the implantation site and engulf the surface of the implant before bone-forming cells, such as mesenchymal stem cells reach there. Consequently, instead of a direct connection between the implant and bone, fibrous tissue encapsulates the surface of the implant creating weak physical contact and low stability allowing the micromotions of the indwelling implant. This sooner or later causes the failure of the implant because the micromovements of the implant owing to the

inappropriate transmission of the loading forces of mastication triggers local bone resorption and implant loosening (114).

2.4.3 Infection of osseointegrated implants

Peri-implant mucositis was defined by Robertson *et al*. as an inflammatory process around a functioning implant characterized by bleeding on probing (BOP) with probing depths of 4 mm or more. With this diagnosis, there is no sign of bone loss other than what would be expected owing to normal marginal bone loss, and it may or may not be accompanied by suppuration. Concerning its prognosis, peri-implant mucositis may be reversible with conservative therapy. Although peri-implant mucositis is generally considered as the precursor of peri-implantitis, some clinical experiences suggest that it may not progress even it is left without treatment. Another difficulty of the objective differential diagnosis is that there is not an evident borderline between the two clinical pictures, the transition from peri-implant mucositis to peri-implantitis may not be characterized by well-defined stages (115, 116).

Peri-implantitis is a specific term to describe an inflammatory process around indwelling implants after successful osseointegration that manifests in gingival inflammation, bone loss around the implant, pocket formation, bleeding on probing with a blunt instrument and suppuration. Although, peri-implant disease can progress without any sign of implant mobility, when it occurs it indicates the complete failure of the implant that has to be removed sooner or later. It is important to note that peri-implantitis is preceded by the undisturbed osseointegration of the implant; peri-implantitis is a consequence of a bacterial infection and the associated bone loss around the implant that may not be attributed to any other known reason (see primary vs secondary peri-implantitis below). The shape of the bone defect is crater-like around the implant and it is more extensive and deeper than it is expectable taking into consideration the normal rate of marginal bone loss. The normal rate of marginal bone loss around the implant is not supposed to be more than 0.2 mm per year (117).

The description of the clinical picture that is referred as peri-implantitis in the scientific literature often varies in a wide-range. This might be because of the lack of a widely accepted exact definition of peri-implantitis in terms of diagnostic parameters

(118). Therefore, the diagnostic parameters that are used for the description of the clinical picture of peri-implantitis vary on a broad spectrum, as well. However, it might be more important to understand the aetiology of peri-implantitis than approaching the question from perspective the development of the definitions that precisely describe the various stages of the clinical picture. From an etiological point of view, the literature distinguishes primary and secondary peri-implantitis. Primary peri-implantitis is defined as an inflammation around the indwelling implant that is caused by the bacterial infection of the surface of the implant without any other known causative reason. In contrast, secondary peri-implantitis is described as a bacterial infection of the indwelling implant but there are other known causatives that are responsible for the clinical picture. Non-bacterial events, like implant overload, implant fracture, residual cement on the surface of the indwelling implant, micro gaps between the implant and the abutment, and poor prosthetic works with uncleanable parts may all be the causatives of secondary peri-implant infections (119).

2.4.4 Causatives of secondary peri-implantitis

The long-term survival of dental implants is supposed to be strongly related to the appropriate angle of loading. Axial loading supports the physiologic bone remodelling that allows the proper transmission of mastication forces from the indwelling implant to the surrounding bone. If the angle of the loading significantly deviates from axial it triggers pathologic bone remodelling ending up in bone resorption around the implant (120, 121). In most of the cases, the availability of sufficient bone volume is the only decisive factor of implant placement, while the positioning of the connecting prosthetic restorations is rarely taken into consideration in the course of the planning that may result in the transmission of mastication forces from inappropriate angles. It must be noted that there is no agreement on the tolerable angle of implant loading. In practice, often the maximum angle of loading is applied that is tolerable by the material of the abutment. Consequently, crater-like bone voids develop around the implant neck triggering the inflammation of the gingiva (122). Owing to the inflammation the biological sealing weakens around the implant neck allowing the invasion of the bacteria from the oral cavity that contaminate the surface of the implant and the surrounding bone tissue. In this stage, the progress of the infection cannot be stopped unless the causative is eliminated.

Antibiotic therapy may only provide a temporary solution because the inappropriate loading of the implant will open the way for the infection over and over. The loading from an extreme angle may lead to the fracture of the implant (123). The fractured implant must be removed surgically from the bone because it loses its function but facilitates bacterial infections.

The quality of prosthetic restorations can have an effect on the development of peri-implant diseases. The prosthetic work might have, for example for aesthetic reasons, a quite uncleanable part, or if the compliance of the patient is not good enough when cleaning the prosthesis, plaque can accumulate on the neck of the implant and lead to peri-implant mucositis and peri-implantitis later on. The method of fixing of prosthetic work on implants may be another causative of peri-implant infections. Luting cement is often used to connect the prosthetic part to the implant. If residual cement is not removed properly and removes under the gingiva it can cause local inflammation and serves as a scaffold for bacterial attachment (115).

Prosthetics with inappropriate geometry or positioning have parts that are not available with cleaning devices allowing the development of plaques (124). The plaques contain substantially the same bacterial strains that play a role in primary peri-implant infections, but the elimination of the causative, that is the uncleanable surface, renders the clinical picture manageable. In this case, the causative of peri-implantitis is the uncleanable surface of the prosthetic part.

If the implant body and the abutment are not precisely connected then gap remains between them allowing micro-motions in the course mastication (122). The gap gives room for the attachment and proliferation of bacteria, whereas the micro-motions transmit pathologic forces resulting in the resorption of the surrounding bone. The bacteria will infect the site of the developing bone void leading to the identical clinical picture then it is in the case of implant loading from an inappropriate angle. The infection cannot be eliminated without the replacement of the imprecisely connecting implant parts.

2.4.4.1 The epidemiology of peri-implant infections

Although there are several publications on the incidence and prevalence of peri-implantitis, because of the lack of unambiguous definition of peri-implantitis and the demarcation of the underlying primary and secondary processes the published values vary between extremes, like 5% to 63,5% (125).

In addition, medical records, which should be the main sources of epidemiological data, are not standardized in terms of quality and quantity of clinical data to be documented and do not disclose the presumable and/or known causatives of peri-implant diseases. Consequently, the medical records are written rather intuitively than objectively making the credibility of the available epidemiologic data questionable. It must also be noted here that medical records may be biased if complications associated with an implant are diagnosed by the same doctors who have provided the treatment beforehand. Research findings suggest that the judgment of doctors is more yielding when it comes to the evaluation of the clinical outcome of their own work than it is in relation to the work of their colleagues (126-128).

In scientific literature, the success of an implant is often described by its 1 to 5 years long survival. Survival is characterized by the uneventful function of the indwelling implant without pain or any discomfort of the patient; however, this approach may not be fully appropriate. Peri-implantitis can progress until severe stages without any symptom, such as pain or bleeding. When the symptoms emerge the peri-implantitis is already in advantaged stage. Nevertheless, the associated bone loss, even if the peri-implantitis remains undiagnosed does not lead to the loss of implant stability even after 5 years of the placement of the implant. Frasson *et al.* demonstrated that the bone loss in the first year of peri-implantitis was 1.62 ± 0.32 mm. In the following years, the rate of bone loss was non-linear, and it never exceeded 6mm even after 5 years. Taking into consideration that the average length of an implant is about 10-14mm, thus the 6 mm loss of the surrounding bone does not result in implant loosening, usually. Nonetheless, if and until the peri-implantitis and the associated bone loss does not cause symptoms/complications for the patient the implantation regarded successful according to the current approach. It is also noted that it is assumable that a significant fraction of peri-implantitis cases remains unknown because of the lack of compliance of patients who are reluctant to

attend medical controls. In conclusion, the long-term follow-up patients who received dental implants would be essential in longitudinal studies to obtain credible data on the epidemiology peri-implantitis (119).

2.4.4.2 Ethical barrier to gather objective epidemiological data on peri-implantitis

In the course of the preparation of medical records, the medical staff is required to pay attention to the sufficient documentation of the clinical picture. The medical records are supposed to be objective, especially if the clinical picture is a presumed complication that is associated with an earlier intervention of other professionals. In general, the medical diagnosis is supposed to be the objective documentation of a clinical picture by using terms that are comprehensible and unambiguous for professionals who work in the same domain. Nevertheless, the explanation of the cause and effect relationship on the medical record is prohibited by medical ethics. There is an exemption from this if the disclosure of the causal relationship between the clinical picture and the causative is related to the own work of the diagnostician. However, this rarely happens owing to the fear of detrimental consequences. But if the complication may be associated with an earlier intervention of another professional the diagnostician is not allowed to extrapolate to the causative reason of the clinical picture, but the objective diagnosis should be recorded, only. For example, if cement pieces are identified in the sulcus based on X-ray and the pieces are removed afterward providing objective evidence of cement leakage in the course of the fixation of the crown, not more than the following diagnosis may be recorded: 'peri-implantitis, foreign material in the sulcus'. Obviously, without the analysis of the chemical composition of the foreign body, the dentist cannot be sure that it is cement or other material. But even if it is cement only forensic dentists have the right to state that the clinical picture, that is, peri-implantitis is the consequence of an earlier inappropriate intervention.

This practice makes sense though, but it also elevates barrier for the comprehensive documentation of the clinical picture making impossible to reveal the underlying reasons of secondary peri-implantitis for epidemiology studies. Ideally, this barrier might significantly be lowered by a guideline on medical records that provide

clear instructions on the extent and depth of clinical data to be documented to support not only the disease management but the epidemiology studies, as well.

2.5 Improvement of the antibacterial property of dental implants

There are various strategies and methods in place to improve the antibacterial attribution of dental implants (Figure 4). In my doctoral work I was studying polymer embedded silver and TiO_2 nanoparticles.

2.5.1 Polymer coatings

Various synthetic polymers have been tried as dental implant materials because they have an aesthetic appearance, their elastic modulus is close to that of soft tissues, it is relatively easy to work with them compared to metals and they are more affordable than titanium (8, 129).

Despite the several advantageous properties, polymer-based dental implants have never been brought to the market. Although the number of publications is limited on this domain; based on the available data it is assumable that synthetic polymers, at the current level of technology, may not be able to bear the mechanical forces of mastication, which might explain their ignoration as implant materials (8). Synthetic polymers are rarely regarded as potential coating materials of dental implants, as well. In the course of systematic literature search, only two papers have been found whose objective was the pre-clinical testing of polymer coatings. Smeets *et al.* developed a nano-silver containing polymer that showed antibacterial property in porcine model, albeit its osseointegration was poorer compared to the SLA control surface (130). Besides that, Slenters *et al*. demonstrated the *in vitro* antibacterial property of a silver containing L-¼ ethanediyl bis(isonicotinate)-based polymer on the surface of titanium against *S. Sanguinis* (131). No further relevant publication was found.

2.5.2 Coating of implant materials with antibacterial nanoparticles

Antibacterial coatings on medical devices have recently been in the focus of research. Because of the overuse of antibiotics and the consequential spread of antibiotic-resistant bacterial strains, new approaches are being searched for preventing and treating infections that occur around implantable medical devices. Antibacterial surfaces are supposed to prevent bacterial attachment or kill bacteria that come to contact with the surface. Depending on the underlying mechanism of action two antibacterial surface types have been defined, i.e. anti-biofouling and bactericidal surfaces (132). Anti-biofouling surfaces usually characterized by special topography that prevent bacterial attachment and so biofilm formation. In contrast, bactericidal surfaces instantly kill bacteria upon contact. Ideally, an antibacterial surface of an implantable medical device has selective toxicity for pathogenic microorganisms, while it does not influence the physiologic function of stromal cells (133).

2.5.3 Medical use of silver and TiO_2 nanoparticles

In the dental material industry, TiO_2 is mostly known for the biocompatible surface of titanium implants. Currently, TiO_2 nanoparticles (NPs) are mostly investigated in resin-based composite materials and ceramics that are used for restorations, which are in contact with the oral cavity and oral mucosa (134-136). TiO_2 NPs are present in bleaching materials and toothpaste, too (137). TiO_2 NPs may also be used as antibacterial agents because of their strong oxidation activity and superhydrophilicity (138). In addition, the photocatalytic property of TiO_2 NPs is utilized in many fields of the industry, like water and air purification and for self-cleaning surfaces, however, this feature remained untapped in medical applications.

Silver nanoparticles (AgNPs) have already carefully been used in medical applications. Currently, AgNPs are mainly used externally in contact with skin or mucosa, like surgical sutures, wound dressings or surgical meshes. Concerning dental applications, AgNPs are components of poly-methyl-metachrylate (PMMA) removable dentures, silicon-based soft reliners and orthodontic adhesive materials that are or may

be in contact with the mucosa in the oral cavity. We can find AgNPs in bisGMA-TEGDMA based filling materials that can interact with dental pulp, and in endodontic rinsing solutions that can interact with the bone and the periodontal ligaments (48). Beside dental applications, there are more invasive applications of AgNPs, like coatings on the surface of central venous catheters and urinary catheters with the aim at preventing infections (48, 139).

2.5.4 Antibacterial property of silver nanoparticles

The practical relevance of AgNPs as antibacterial agents derives from the problem of the spreading antibiotic resistance of pathogenic bacteria. Silver ion has innate wide-spectrum antibiotic property that may make it a good candidate as an alternative or complementary substance to the currently available antibiotics. The antibacterial property of AgNPs may be influenced by the size and the physicochemical properties of the nanoparticles, and the type of bacteria (139). Recent findings suggest that under *in vitro* experimental conditions the antibacterial effect of AgNPs may be related to the cellular uptake of the NP by the bacteria. This mechanism assumes that AgNPs exert their cytotoxic effect intracellularly causing oxidative stress by the release of free radical (139).

Recently, it has been observed that immobilized AgNPs may retain their bactericide behaviour. This phenomenon is referred as contact antibacterial property of AgNPs that are permanently anchored to the surface of a bulk material. The nanoparticles dramatically increase the surface area of a bulk material creating high contact area to attack the bacterial cell wall. Contact of the bacterial membrane and the AgNP results in physical damages of the cell wall. AgNPs can anchor to the cell wall, infiltrate it and this leads to bacterial damage and cell death. The findings of electron spin resonance spectroscopy studies suggest that the anchored AgNPs retain their ability to trigger the formation of ROS that are responsible for the destruction of the bacterial cell wall and membrane (140, 141). Agnihotri *et al*. showed that immobilised AgNPs show stronger antibacterial effect than silver plates and silver colloid (142).

AgNPs are in focus of recent researches for improving the antibacterial properties of the surface of dental implants. The known studies are mostly in pre-clinical stage, very few clinical studies are available (based on database search). Juan *et al*. developed AgNP containing titanium surfaces that were effective against *Staphylococcus aureus* and *Escherichia coli* in *in vitro* experiment (143). Zhao *et al*. incorporated AgNPs to titanium nanotubes and tested antimicrobial activity against *Staphylococcus aureus* and biocompatibility with primary rat osteoblasts. They found that AgNPs could be good candidates to prevent implant associated infections, but are still not expectable to act as long as needed in smaller doses that are not cytotoxic (144). According to our best knowledge there is no AgNP containing implant surface on the market yet or even in clinical study phase in relation to dental or orthopaedic applications.

2.5.5 Preliminary results of our research team

Other members of our research team developed photochemically and photobiologically active nanocomposite polymers which originally were intended for environmental application such as self-cleaning surfaces (145). Some of them showed considerable *in vitro* antibacterial property that raised the possibility of their medical applications.

Poly(ethyl-acrylate-co-methyl methacrylate) polymer matrix (referred to as p(EA-co-MMA)) was created in which photocatalytic nanoparticles were dispersed. The performance of two photocatalysts were investigated: *i*) P25 TiO_2 nanoparticles (NPs) (Degussa-Evonik), and *ii*) silver nanoparticles (AgNPs) coupled with P25 TiO_2 NPs (Ag-TiO_2). The silver coupling enhances the innate photocatalytic activity of TiO_2 NPs by changing their optical properties and electric structure allowing the absorption of photons in the UV-VIS range (Figure 5). Owing to this feature 90% of *Staphylococcus aureus* colonies could be eliminated from the surface the Ag-TiO_2 containing p(EA-co-MMA) polymer (1.25 mg/cm^2) after 15 minutes illumination by using an ordinary light source having emission in UV-A/VIS range (Figure 6). Interestingly, the TiO_2 and Ag-TiO_2 showed some contact antibacterial property without photoinduction (in dark). Concerning Ag-TiO_2 containing nanocomposite, the authors discerned that the contact antibacterial

property might have been caused by releasing silver ions from the surface of the nanocomposite polymer (Figure 7).

The XPS spectra confirmed the presence of Ti, O and C atoms on laser-ablated surfaces (Figure 8). These elements are typically observed on investigated surfaces and the positions and intensity of the O 1s and Ti 2p peaks prove the presence of an intact TiO_2 layer (146, 147). Trace amounts of Al could also be detected as a result of the process of sample fabrication. In general, the laser treatment altered the surface chemistry in only a few respects. The C 1s signal indicates the presence of carbonaceous contamination presumably because of carbon-containing molecules that remained on the surface after chemical cleaning or adsorbed from the ambient air (148, 149). Representative high-resolution Ti 2p spectra of control and laser-treated Ti samples are depicted in Figure 9. The core level spectrum displays two characteristic peaks, at 458 eV and at 464 eV, corresponding to the positions of the Ti 2p3/2 and Ti 2p1/2 peaks, respectively (Figure 9A). This confirms the presence of an intact TiO_2 layer on the control samples (149). For the Nd:YAG laser-treated samples, two shoulders appear at binding energies of 454.7 and at 456.5 eV (Figure 9B). These can be assigned to Ti^{3+} and to metallic titanium (150). This suggests that, besides a thin TiO_2 layer, Ti^{3+} and metallic forms of titanium are present on the Nd:YAG laser-treated samples. In the case of the excimer laser irradiated samples only a small shoulder can be observed at 456.9 eV (Figure 9C) (13).

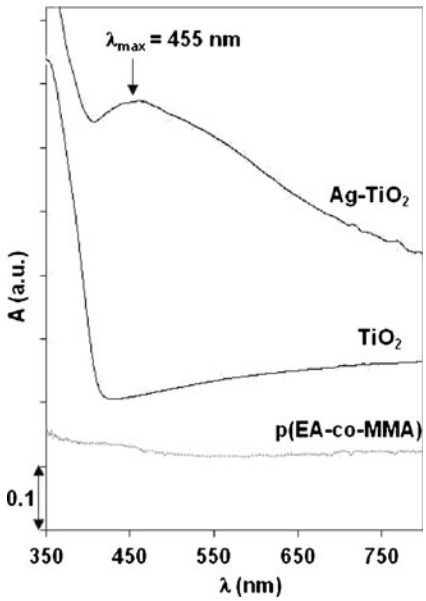

Figure 5 shows the UV-VIS absorption spectra of TiO_2 and Ag-TiO_2 photocatalysts (without polymer matrix) and p(EA-co-MMA) polymer (without embedded photocatalyst). Owing to the silver photodeposition an absorption band appeared on the spectra between 400 and 550 nm with a maximum of 455 nm, which indicates the plasmonic effect of the silver nanoparticles. Figure and legend are reprinted from reference (145).

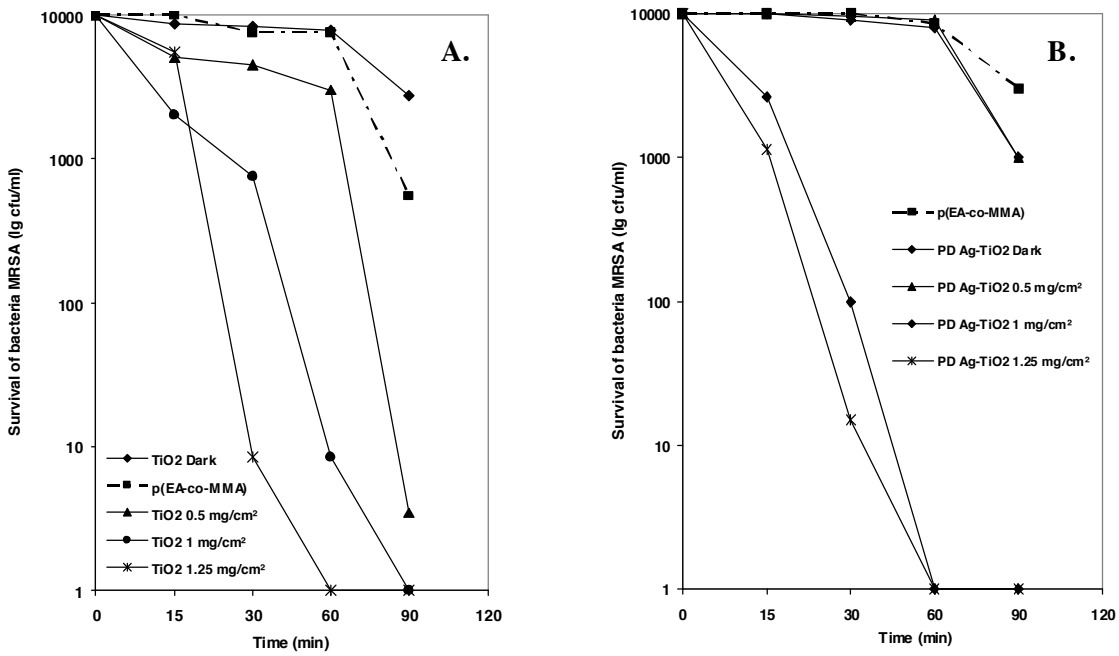

Figure 6 shows the antibacterial activity of p(EA-co-MMA) layers with varying amount (catalyst = 0 – 1.25 mg/cm^2) of TiO_2 (A) and photo-deposited (PD) Ag-TiO_2 (B) photocatalysts against methicillin resistant Staphylococcus aureus under visible light irradiation. It was observed that increasing the catalyst

content in the polymer resulted higher antibacterial activities in both cases. The highest activity was observed at 1.25 mg/cm^2 catalyst surface concentration for both photocatalysts. After 15 minutes of irradiation the Ag-TiO_2 photocatalyst thin layer inhibited the growth of 90% of the bacteria, while TiO_2 inhibited only 80%. The antibacterial tests were performed on films containing 1.25 mg/cm^2 photocatalyst under dark condition for reference. The results revealed that the bactericidal effect was more pronounced under light irradiation than in dark on TiO_2 and on PD Ag-TiO_2 on both polymers. Figure and legend are reprinted from reference (145).

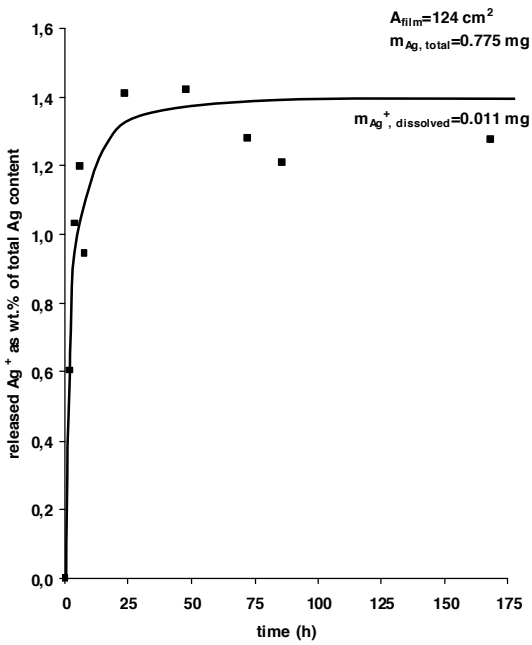

Figure 7 shows the percentile amount of dissolute Ag^+ released from p(EA-co-MMA) based Ag-TiO_2 catalyst film (Afilm= 124 cm^2, 1.25 mg/cm^2 specific catalyst content). Figure and legend are reprinted from reference (145).

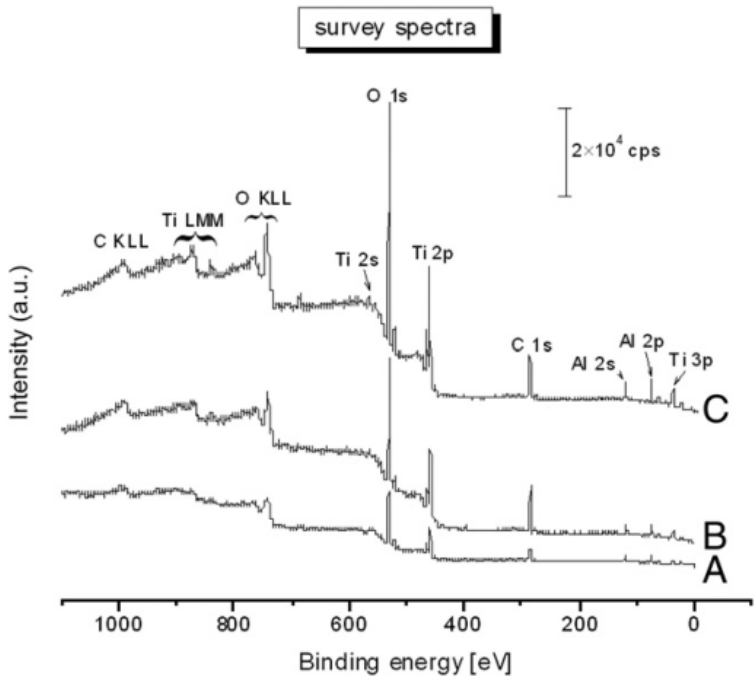

Figure 8 shows the representative XPS spectra of (A) sandblasted/acid-etched surface (control), (B) a Nd:YAG laser-ablated surface (200 laser shots at a fluence of 1.3 J/cm^2, FWHM = 10 ns) and (C) a KrF excimer laser-modified surface (2000 pulses, FWHM = 18 ns, fluence = 0.4 J/cm^2) (151).

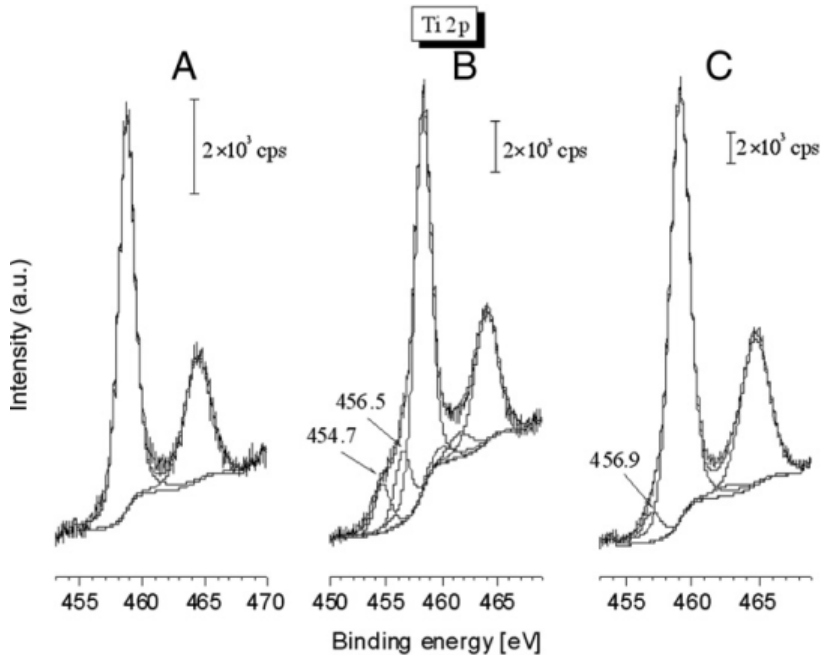

Figure 9 shows the representative high-resolution XPS spectra with Ti 2p lines concerning (A) control, (B) Nd:YAG laser-treated and (C) a KrF laser-treated surfaces (151).

2.5.6 Photocatalytic activity of TiO_2 nanoparticles

Typically, TiO_2 is an n-type semiconductor because of oxygen deficiency. The band gap is 3.2ev for anatase and 3.0 for rutile. They are the two most often polymorphs of TiO_2 (152). In photocatalysis, electromagnetic radiation, e.g. light of energy greater than those band gaps excites an electron from the valance band to the conduction band. The excitation of an electron to the conduction band creates a positive hole in the valance band. Charge carriers, i.e. positive holes and excited electrons initiate redox reactions through the oxidation of adsorbed H_2O and organic molecules creating reactive oxidizing species (ROS), like hydroxide and organic radicals. This mechanism may be responsible for the photocatalytic degradation of absorbed organic compounds, such as pyrogens and bacteria (Figure 10) (153).

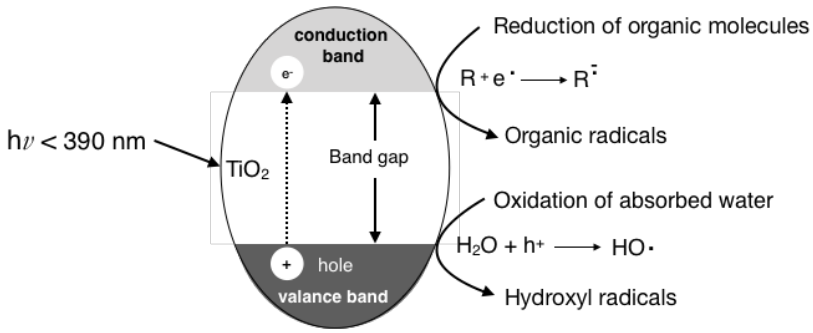

Figure 10 shows the scheme of TiO_2 photocatalytic mechanism**.** Incident UV light excites an electron (e^-) from the valance band to the conduction band of TiO_2. The charge carriers (positive hole and electron) initiate redox reactions via two simultaneous events: 1.) excited electron reduces surrounding electron acceptors, such as absorbed organic molecules; 2.) the photogenerated positive hole oxidizes the dissociatively absorbed water molecules. These reactions lead to the production of hydroxyl and organic radical anions that are responsible for photocatalytic reactions. The figure is an adaptation from reference (152).

2.5.7 UV-VIS activated photocatalysis of Ag coupled TiO_2 nanoparticles

Coupling of TiO_2 or deposition of silver on the surface of TiO_2 semiconductor significantly enhances the photocatalytic efficiency even under visible light by decreasing

the recombination rate of the photogenerated electron-hole pairs. When recombination occurs, the excited electron reverts to the valance band without reacting with the absorbed molecules. Silver acts as an electron trap, promoting interfacial charge transfer which lengthens the lifetime of charge carriers and therefore increases the chance for the production hydroxyl and organic radical anions (Figure 11). Gunawan *et al*. demonstrated the reversible photoswitching of nanosilver on TiO_2 where reduced silver on a TiO_2 support exposed to visible light (> 450 nm) resulted in excitation and reverse electron flow from silver to TiO_2 support, oxidizing silver ($Ag^0 \rightarrow Ag^+$) in the process. The visible light responsiveness was attributed to the surface plasmon resonance of silver nanoparticles (152).

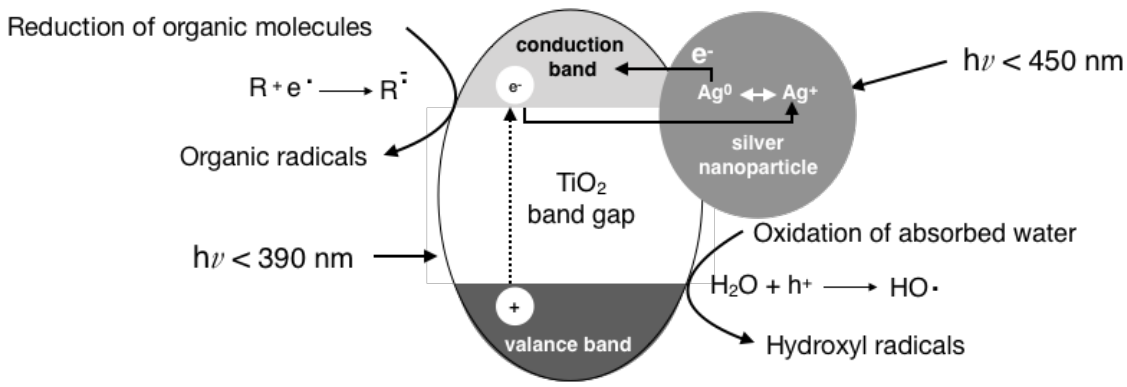

Figure 11 shows the overall scheme of the reversible and cyclic photoswitching of silver nanoparticles on TiO_2. The visible component of the incident light excites an electron from metallic silver (Ag^0) that flows to the conduction band of TiO_2 and reduces adsorbed electron acceptor organic molecules. The ultraviolet component of the incident light excites an electron from the valance band to the conduction band of TiO_2. The excited electron reduces Ag_2O back to metallic state ($Ag^+ + e^- \rightarrow Ag^0$) by reverse electron flow from TiO_2 towards the coupled silver nanoparticle. The positive hole in the valance band of TiO_2 oxidizes the absorbed water molecules yielding hydroxyl radicals. The figure is an adaptation from reference (154).

3 OBJECTIVES

The long-term survival of dental implants is compromised by peri-implantitis. There are two approaches to prevent this:

1.) Ensuring gap-free epithelial sealing around the implant to prevent the invasion of bacteria from the oral cavity;
2.) Improvement of the antibacterial property of the surface of dental implants.

3.1 Investigation of the *in vitro* biocompatibility of prosthetic materials with human epithelial cells

The prerequisite of the prevention of primary peri-implantitis that is caused by bacterial invasion from the oral cavity is the adhesion of epithelial cells around the cervical part of the prosthetic abutment and the neck of the implant creating gap-free biological sealing. Various prosthetic materials have been in clinical use, but little is known about their biocompatibility with epithelial cells.

The first objective of the present doctoral work was to investigate the *in vitro* biocompatibility of prosthetic materials.

3.2 Investigation of the *in vitro* biocompatibility of laser ablated TiO_2 surfaces

Various strategies and technological approaches have been applied in order to create TiO_2 surfaces of various roughness on titanium dental implants. The smoother TiO_2 surfaces facilitate the attachment of epithelial cells and so the development of epithelial sealing, while rough surfaces are supposed to support the secondary stability of the indwelling implants. In principle, the higher the secondary stability of the implant the lower the risk of micromotion induced secondary peri-implantitis. Laser ablation has been regarded as an innovative method that allows good control over the production of uneven TiO_2 surfaces on titanium implants.

The second objective of the present doctoral work was to investigate the *in vitro* biocompatibility of laser ablated TiO_2 surfaces.

3.3 Investigation of the *in vitro* antibacterial property of nanocomposite polymers

TiO_2 surfaces with increased roughness are beneficial for the secondary stability of dental implants, albeit such surfaces show increased proneness for bacterial infections. The micro-size ditches and pits help the attachment of sporadic early-colonizer bacteria, which by multiplying themselves and producing biofilm may engulf the entire surface of the implant.

The third objective of the present doctoral work was to investigate the contact and photocatalyzed antibacterial property of polymer embedded TiO_2 and silver coupled TiO_2 nanoparticles on the surface titanium implant materials.

4 MATERIALS AND METHODS

4.1 *In vitro* biocompatibility of prosthetic materials with human epithelial cells

4.1.1 Preparation of samples of prosthetic materials

Cylindrical samples of 1.5 mm height and 9 mm diameter were prepared from lithium-disilicate (IPS e.max Press, Ivoclar Vivadent AG Germany), yttrium modified zirconium dioxide (5-TEC ICE Zirkon Translucent, Zirkonzahn GmbH Srl, Germany) and CoCr alloy (Remanium star, Dentaurum GmbH & Co. KG, Germany). Before examination, the samples (n = 20) were cleaned ultrasonically in 70% ethanol, each for 15 min and subsequently rinsed in ultrapure water. The experiments with human epithelial cells were carried out on 5 samples per type at a time and experiments were repeated 4 times (155). As positive control, the proliferation of cells was measured in culture plates (data not shown). The justification of the relevance of the selected test materials is shown in Table 5 based on their clinical role.

Table 5 shows the clinical relevance of the selected test materials.

Material	Clinical role
CoCr alloy	Base material of porcelain fused metal crowns that is the most used material for fixed (crown and bridge) restorations
Lithium-disilicate	Most frequently used metal-free aesthetic material for crown and short bridge restorations
Yttrium modified zirconium dioxide	Used as restorative and also implant material. Metal free solution for crowns and even full arch bridges.

4.1.2 Culturing of human epithelial cells

Adult epidermal epithelial cells were isolated and cultured from inflammation-free oral mucosa of one healthy donor (age 18–46) undergoing dento-alveolar surgery. The protocol of the experiments was approved by the Human Investigation Review Board of the University of Szeged (N° 130/2009). Complying with all ethical standards of

research in accordance with the Helsinki Declaration the subject enrolled in the research provided signed informed consent.

Mucous membrane specimens were first washed in SalsolA solution (Human Rt, Gödöllő, Hungary) supplemented with 2% antibiotic, antimycotic solution (Sigma–Aldrich GmbH, Germany). Overnight incubation in dispase solution (Grade II, Roche Diagnostics, Mannheim, Germany) was carried out at 48°C to separate the dermis from the epidermis (156). The following day, the epidermis was peeled off the dermis. The epidermis was then placed in 0.25% trypsin-EDTA solution (Sigma–Aldrich GmbH, Germany) for 5 min at 37°C. Following trypsinization, the epidermis was taken apart mechanically and washed vigorously to release epidermal cells. The epidermal cell suspension was centrifuged at 200 × g for 10 min at 4°C. The epidermal cells were then placed in 25 cm^2 tissue culture dishes (Orange Scientific, Belgium). The oral epithelial cell culture medium consisted of keratinocyte serum-free medium with L-glutamine (Gibco BRL, Eggstein, Germany), supplemented with recombinant epidermal growth factor 2.5 mg/500 ml (Gibco BRL, Eggstein, Germany), bovine pituitary extract 25 mg/500 ml (Gibco), L- glutamine and antibiotic/antimycotic solution containing penicillin G sodium 1%, streptomycin sulphate 1% and amphotericin B 0.0025% (Sigma–Aldrich GmbH, Germany). Fresh culture medium was added to the cells three times per week. The primary epithelial cell cultures reached ~ 90% confluence in 8–16 days. Confluent primary cultures were treated with phosphate-buffered saline (pH = 7.4, Gibco BRL, Eggstein, Germany) and cells were harvested by a 2-4 min trypsinization with 0.25% trypsin-EDTA solution (Sigma–Aldrich GmbH, Germany). Harvested cells were divided into 2–4 equal parts at passages. Cultures were grown at 37°C in a humidified atmosphere containing 5% CO_2 (155).

4.1.3 Investigation of the proliferation of epithelial cells on prosthetic materials

AlamarBlue (AB) is a nontoxic, nonradioactive, water-soluble, readily detectable indicator dye used in a cell viability assay developed to measure the proliferation of various human and animal cell lines, bacteria and fungi. It incorporates a redox indicator that both fluoresces and changes colour in response to the chemical reduction of the

growth medium resulting from cell growth. The living cell number was determined through the reduction of resazurin with absorbance-based instrumentation. Cells were cultured on the discs in 48-well plates at a density of 10^4 cells/well. The culture medium was changed to RPMI 1640 medium without phenol red (PAA Laboratories GmbH, Austria) after 24h or 72h with AB (AbDSerotec, United Kingdom) added at a final concentration of 10% according to the manufacturer's recommendations, and the cells were incubated for three and a half hours under standard culturing conditions. OD_{570} and OD_{600} were measured by a Multiskan Spectrum spectrophotometer (Thermo Labsystems, Vantaa, Finland) and Skanit Software 2.4.2 RE (Thermo Labsystems, Vantaa, Finland). The summary of the experimental setting is shown in Table 6.

Table 6 shows the experimental setting of the biocompatibility test of restorative dental materials.

Materials	Cell type	Assay
Lithium-disilicate	Human oral mucosa derived epithelial cells	Alamar Blue
Yttrium modified zirconium dioxide		
CoCr alloy		

4.1.4 Statistical analysis

The proliferation of adhered cells was expressed as the percentage change in the reduction of AB, which was calculated from the OD_{570} and OD_{600} values for each well according to the protocol provided by the manufacturer. After normality testing the data were compared via one-way analysis of variance (ANOVA), followed by the LSD, Sidak and Dunnett post hoc tests to determine statistical differences after multiple comparisons (SPSS 17.0, IBM Corporation, Armonk, NY, USA). Comparison of the 24h (attachment) and 72 h (proliferation) observations was carried out with Student's t-test for paired samples. A probability value of $p < 0.05$ was considered as statistically significant (155).

4.2 *In vitro* biocompatibility of laser ablated TiO_2 surfaces

4.2.1 Preparation of titanium discs

For the experiments 1.5 mm thick, 9 mm in diameter discs were cut from commercially pure (CP4) titanium rods (Daido Steel, Japan). After degreasing the discs were subjected to sandblasting with aluminium oxide of 150 µm grain size (FINO, Germany) and then to acid etching with nitric acid (Reanal, Hungary). Before further processing the samples were cleaned ultrasonically in acetone then in 70% ethanol for 15 min and finally rinsed in ultrapure water (13, 151).

4.2.2 Surface ablation with a Nd:YAG laser

A frequency-doubled Q-switched Nd:YAG laser (Guangzhou Gabriel Optic-Electronic Co., Ltd, China; λ = 532 nm, FWHM = 10 ns) was used for the ablation of titanium discs (n = 80). In the first experiments, two parameters were varied independently. The incident fluence was varied in the range 1-1.5 J/cm^2, and the laser energy was adjusted by placing neutral filters in the beam path. The surface modifications were performed with 200, 300 or 400 shots of pulses. The optimal fluence and the number of laser pulses were then selected based on the preliminary SEM measurements: the visible beam was imaged onto the surface of the samples by a fused silica lens (f = 10 cm) and the applied fluence was 1.3 J/cm^2. A 3.6 mm^2 area on the sample surface was illuminated by a series of 200 laser pulses under atmospheric conditions. The beam energy at the target surface was monitored by the display of the laser using a calibration curve (13).

4.2.3 Surface ablation with a KrF excimer laser

Further experiments were performed with a ns KrF excimer laser beam (LLG

TWINAMP, Laser Laboratorium, Göttingen, Germany, λ = 248 nm, FWHM = 18 ns), using fluence in the interval 0.4-0.6 J/cm^2, and a number of pulses ranging from 500 to 2000. A square aperture that cut out the most homogeneous part of the beam was imaged onto the surface of the titanium samples by a fused silica lens with a focal length of 20 cm. As in the case of the Nd:YAG laser treatment, the optimal fluence and the number of laser pulses were selected on the basis of the preliminary SEM measurements. The applied fluence on the titanium surface was 0.4 J/cm^2, the illuminated area was 10.5 mm^2 and the number of pulses was 2000 under atmospheric conditions. The laser beam energy at the sample was monitored by calibrated energy measurement of a reference beam, coupled out by a fused silica plate. In total, 80 discs were treated (13).

4.2.4 Microscopic investigations of the laser ablated titanium surfaces

The surface structure of the samples was first observed by means of an optical microscope (Nikon Eclipse 80i, Japan). High-resolution secondary electron images were then recorded with a scanning electron microscope (Hitachi S4700, Japan). For better spatial visualization of the structures all samples were tilted at 75° during SEM.

For quantitative surface roughness determinations atomic force microscope (AFM) was applied (PSIA XE-100 instrument, PSIA Inc., South Korea). The tips were single-crystal silicon cantilevers (type: N, NSG01 series with Au conductive coating, resonant frequency 87-230 kHz, force constant 1.45-15.1 N/m) purchased from NT-MDT (Russia). The measurements were performed in tapping mode, and the height, deflection and 3D images with areas of 10 × 10 µm and 5 × 5 µm were captured. Ra values were determined as the arithmetic average of the surface height relative to the mean height by the AFM software program on the basis of at least 6 independent measurements (13).

4.2.5 Culture of osteoblast-like MG-63 cells

Osteoblast-like MG-63 cells were obtained from the European Collection of Cell Cultures (157). The frozen ampoule was transferred to a 37°C water bath for 1-2 min. The contents of the ampoule were centrifuged in phosphate-buffered saline (PBS) (PAA

Laboratories GmbH, Austria), and foetal bovine serum (FBS) (PAA Laboratories GmbH, Austria) solution. Harvested cells were pipetted into a 125-cm^2 flask containing 15 ml medium. After 2– 3 days, the culture was confluent and the cells were passaged into 2–4 flasks. The MG-63 cell culture medium consisted of Eagle's minimal essential medium (EMEM) (Sigma-Aldrich GmbH, Germany), 1% glutamine, 1% nonessential amino acids (Sigma-Aldrich GmbH, Germany) and 10% FBS. The MG-63 cell cultures reached ~ 70% confluence in 2– 4 days. Confluent cultures were rinsed twice with PBS (pH = 7.4, Gibco) and the cells were harvested by a 2-4-min trypsinization with 0.25% trypsin-EDTA solution (Sigma-Aldrich GmbH, Germany) with centrifugation. Harvested cells were divided into 6–12 equal parts at passages. Cultures were grown under standard conditions at 37°C under a humidified atmosphere containing 5% CO_2 (13).

4.2.6 Cell attachment and proliferation on laser ablated TiO_2 surfaces

The control and treated titanium discs were cleaned with acetone and then with alcohol and sterilized on both surfaces under UV-C radiation (20 min) before the MG-63 cell culturing experiments. Onto each disc 10^4 MG-63 cells in 0.5 ml medium were seeded in 48-well cell culture plates. The same amount of cells was seeded on wells that did not contain titanium discs. The ideal number of cells to be used per disc was determined in preliminary calibration experiments. Cells representing passage numbers of 12–17 were used for all assays. The cell adhesion was determined at 24h and the cell proliferation at 72h. Four parallel experiments were performed, and 5 samples were used for each treatment and for each assay (13).

4.2.6.1 MTT assay

The growth of cultured MG-63 cells was measured by means of a colorimetric assay which determines the living cell number via the reduction of MTT (Sigma Aldrich GmbH, Germany) (158, 159). Cells were seeded onto the titanium discs in 48-well plates at a density of 10^4 cells/well and grown on the discs in culture medium for 24h or 72h.

The supernatant was removed and replaced with 0.5 mg/ml MTT solution in RPMI 1640 media without phenol red. After incubation for 4h under standard culturing conditions the medium was gently removed from each well and the crystallized formazan dye was solubilized with 0.04M HCl in absolute isopropanol and 10% sodium dodecylsulfate. The optical density of the solution at 540 nm (OD_{540}) was determined with a Multiskan Ex spectrophotometer (Thermo Labsystems, Vantaa, Finland) and Ascent Software (Thermo Labsystems, Vantaa, Finland) (13).

4.2.6.2 AlamarBlue assay

Cells were cultured on the discs in 48-well plates at a density of 10^4 cells/well. The culture medium was changed to RPMI 1640 medium without phenol red (PAA Laboratories GmbH, Austria) after 24h or 72h with AB (AbD Serotec, United Kingdom) added at a final concentration of 10% according to the manufacturer's recommendations and the cells were incubated for 3.5h under standard culturing conditions. OD_{570} and OD_{600} were measured by a Multiskan Spectrum spectrophotometer (Thermo Labsystems, Vantaa, Finland) and Skanit Software 2.4.2 RE (Thermo Labsystems, Vantaa, Finland) (13, 160).

4.2.7 Investigation of osteogenic differentiation on laser ablated TiO_2 surfaces

Onto the surface of the discs 10^4 MG-63 cells in 0.5 ml osteogenic differentiation media were seeded in 48-well plates. Osteogenic differentiation media consisted of MEM-α, 15% FBS, 10^{-8} M dexamethasone, 50 µg/ml L-ascorbate phosphate, 5 mM β-glycerophosphate, and 1.8 mM monopotassium phosphate. Cells were incubated for 3 or 7 days in 37°C air containing 5% CO_2. ALP activity was determined by the hydrolysis of p-nitrophenyl phosphate in 2-amino-2-methyl-1-propanol buffer, pH 10.4, at 37°C for 30 min. Absorbance was measured at 504 nm wavelength with a Multiskan Ex spectrophotometer (Thermo Labsystems, Vantaa, Finland) and Ascent Software (Thermo Labsystems, Vantaa, Finland) (151).

4.2.8 SEM investigation of cells on laser ablated TiO_2 surfaces

SEM measurements were performed on two samples of each sort of surface modification. After the cleaning process the discs were sterilized thermally. Cells were placed on the discs at a density of 10^4 cells in culture media. Attachment was observed after 24h. The samples were subsequently dehydrated in graded ethanol and acetone and dried in critical point dryer (type SPI 1320). Mounted specimens were gold-coated by using an Edwards sputter coater and investigated by scanning electron microscope (Hitachi S 2400) (13).

4.2.9 Statistical analysis

The arithmetic means ± the standard error of the mean ($\sigma_{\bar{x}}$) were calculated for the Ra (nm) values measured by AFM. For the MTT method, the mean $OD_{540} \pm \sigma_{\bar{x}}$ is given. In the AB method, the percentage reduction of AB was calculated from the OD_{570} and OD_{600} data by the given protocol. After normality testing the data were compared via one-way analysis of variance (ANOVA), followed by the LSD, Sidak and Dunnett post hoc tests to determine statistical differences after multiple comparisons (SPSS 17.0, SPSS, Chicago, Illinois, USA). A probability value of $p < 0.05$ was considered to be statistically significant (13).

4.3 *In vitro* antibacterial property of nanocomposite polymers

4.3.1 Preparation of Ag/TiO_2/polymer nanohybrid coatings on titanium discs

As a starting material, standard photocatalyst TiO_2 (Degussa P25, Evonik, Germany) with a specific BET surface area of 50 m^2 /g was used without any treatment. In the first step of the preparation, Ag nanoparticles were placed onto the surface of TiO_2 by photodeposition. In this process TiO_2 powder was dispersed in $AgNO_3$ (Molar, Hungary)

solution to obtain Ag-TiO_2, then 2-propanol (Molar, Hungary) was added as a sacrificial donor to promote the photoreduction of Agþ ions under UV light illumination by a 300 W Xe-lamp (Hamamtsu L8251, Japan) under 1 h continuous stirring. The prepared Ag-TiO_2 photocatalyst contained 0.5 wt% surface silver nanoparticles. The detailed process of the Ag-TiO_2 synthesis was described in our earlier publications (161). Dodecyl-sulfate (DS) surfactant molecules were used in 10 wt% to provide hydrophobic character to the photocatalyst particles and increase the dispersibility of the originally hydrophilic photocatalyst particles in the polymer film. The hydrophobically modified TiO_2 and Ag-TiO_2 samples were denoted as DS-TiO_2 and Ag-DS/TiO_2, respectively. During the preparation of the DS-TiO_2 and AgDS/TiO_2 photocatalysts the negatively charged surfactant molecules were added to the positively charged TiO_2 suspension at pH = 4.0. The photocatalysts were washed four times then dried and pulverised.

The photocatalysts were then added to poly(ethyl acrylate-co-methyl methacrylate (p(EA-co-MMA)) solution to yield photocatalyst/polymer mass ratios of 60:40. In order to avoid phase separation 2% polyacrylic acid was added to the dispersion as a chemical stabilizer. The polymer/photocatalyst dispersion was next sonicated for 30 minutes and sprayed onto the surface of the titanium discs using an AD-318 spray gun (Alder, USA). Sandblasted/acid etched titanium discs were prepared according to the protocol detailed earlier. The resulting film coating was dried to a constant weight (3 ± 0.1 mg/cm^2) at elevated temperature (~120 °C). The detailed process of the synthesis was published in our earlier publications (145). After the preparation of the coating layers the discs were sterilized in a hot air sterilizer at 180°C for 45 min. Finally, the discs were subjected to UVC irradiation at 254 nm wavelength for 60 min in order to decompose the upper layers of the polymer bed to uncover the photocatalyst nanoparticles. After cleaning we had five different types of film on the surface of the titanium discs as they are shown in Table 7 (151). Schematic drawings of the NP containing surfaces are presented on Figure 12.

Table 7. Experimental groups. Dark set comprises the number of samples that were stored in dark, while light set comprises the number of samples that were subjected to UV-VIS irradiation in each experimental group.

Surface types	Group	Dark set	Light set
Sandblasted and acid-etched surface	(A)	n=16	n=16
p(EA-co-MMA) copolymer	(B)	n=16	n=16
60wt% TiO_2 : 40wt% copolymer	(C)	n=16	n=16
60wt% DS-TiO_2 : 40wt% copolymer	(D)	n=16	n=16
60wt% Ag-TiO_2 : 40wt% copolymer	(E)	n=16	n=16
60wt% Ag-DS/TiO_2 : 40wt% copolymer	(F)	n=16	n=16

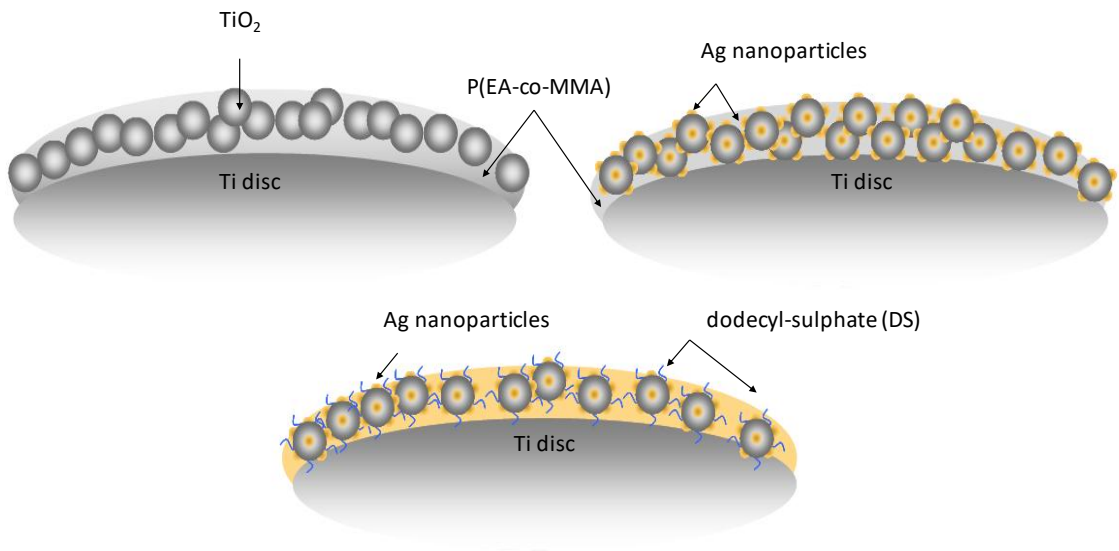

Figure 12. Schematic drawings of the NP containing surfaces. Figure is reprinted from reference (162)

4.3.2 UV-Vis absorption spectroscopy

The determination of the absorption spectra of the composite films was performed with NanoCalc 2000 Micropack spectrophotometer (Ocean Optics, USA) equipped with

an integrated sphere and HPX 2000 Mikropack high power xenon lamp. USB2000 diode array spectrophotometer (Ocean Optics, USA) was applied for the detection of absorbance. (151)

4.3.3 SEM examination of the of Ag/TiO_2/polymer nanohybrid coatings

High-resolution secondary electron images were taken with a scanning electron microscope (Hitachi S4700, Japan) at 500-fold magnification. For the better spatial visualization of the surface structures the discs were rotated by 45° around their longitudinal (y) axis for image acquisition (151).

4.3.4 Roughness measurements of the of Ag/TiO_2/polymer nanohybrid coatings

Profilometry measurements were performed with Veeco, Dektak 8 Advanced Development Profiler® (Veeco Instruments, USA). The tips had a radius of curvature ~2.5 µm and the force applied to the surface during scanning was ~9.8 µN. The image resolution in the x (fast) and y (slow) scan direction was 0.167 µm and 6.35 µm, respectively. The vertical resolution was 40Å. On each sample the surface topography of 500 x 500 µm area was recorded at six different places and the average roughness values (Ra) were calculated. Measurements were performed before and after the UVC irradiation of the surfaces (151).

4.3.5 Contact angle measurements of the of Ag/TiO_2/polymer nanohybrid coatings

Contact angles were measured to examine the wettability of the surfaces before and after UVC irradiation. The wetting properties of the polymer based reactive composite films were investigated by EasyDrop contact angle measuring system (EasyDrop K-100; Krüss Gmbh., Germany). The sessile drop method was applied to

measure the contact angle. The measurements were carried out at room temperature and the contact angle values were determined before and after UVC irradiation (HPA 400/30 SD type lamp; Philips, Hungary) (151).

4.3.6 Isolation and characterization of *S. salivarius*

S. salivarius was chosen as a model bacterium for the experiments because of its significant role as a primary colonizer in peri-implantitis. Clinical isolate of *S. salivarius* was used in this study offered by courtesy of the Institute of Clinical Microbiology, Faculty of Medicine, University of Szeged. The strain was kept at -80°C in Brain Heart Infusion (BHI) broth (Oxoid, UK) containing 12% (v/v) glycerol. The bacteria were cultured for 24 hours on Columbia based agar supplemented with 5% cattle blood (bioMérieux, S.A. Marcy l'Etoile, France) for characterization and further experiments. The characterization of the strain was performed with Microflex LT MALDI-TOF mass spectrometer (Bruker Daltonik, Bremen, Germany). Parameter settings were: linear positive ion mode with laser frequency of 60 Hz, mass spectrometry range 2-20 kDa. The sample preparation was performed by formic acid extraction method. Briefly, a single colony was transferred into an Eppendorf tube and suspended by pipetting up and down in 300µl double-distilled water. Then 900µl 96% (v/v) ethanol was added and the mixture was suspended again. The mixture was centrifuged for 2 min by 13000 r/min. The supernatant was removed, and the pellet was exsiccated at room temperature. The pellet was re-suspended in the compound of 10µl 70% aqueous formic acid and 10µl acetonitrile. After centrifugation 1µl of the supernatant was pipetted onto the MALDI target plate and 1µl of MALDI matrix (a solution of 10mg/ml α-cyano-4-hydroxycinnamic acid in 50% acetonitrile/ 2.5% trifluoro-acetic acid) was added after drying to the sample at room temperature. The acquired data was automatically analysed by MALDI Biotyper 3.1 software and database (Bruker Daltonik, Bremen, Germany). The species-specific identification was performed according to the standard pattern matching approach based on the guidance of the user manual applying log(score) ≥ 2.0 (151).

4.3.7 Antibacterial activity of Ag/TiO_2/polymer nanohybrid coatings

S. salivarius was introduced into 0.5 ml reduced BHI broth (Oxoid, Basingstoke, United Kingdom) in a density adjusted to McFarland standard 0.5. The bacteria were cultured with the coated and the control discs in 48 well plates for 4 hours under standard conditions at 37°C. The growth of *S. salivarius* on the surface of the discs was measured by means of MTT assay (Sigma Aldrich GmbH, Germany) (151).

The coating of the titanium discs by photocatalyst containing polymer changed the optical properties of the surfaces as it was expected according to the preliminary results of the other members of our research team. The absorbance spectra of the coated surfaces is shown in Figure 13. As the result of silver coating, an absorption band appeared on the spectrum between 400 and 600 nm (visible range) with a maximum at 455 nm (151).

In order to investigate the photocatalysis mediated antibacterial property of the polymer nanohybrid coatings the experimental groups were divided into 'light' and 'dark' sets. In the 'light' set the discs were irradiated for 10 minutes at 37°C with UV-VIS light source using a 15W low-pressure mercury lamp with an intensity of 1.26×10^{-6} einstein/s in the VIS range (LightTech, Hungary). It has characteristic emission wavelengths mostly above 435 nm. However, it also has emission lines at 254, 353 and 393 nm but the intensity of these lines is significantly lower compared to that of visible range wavelengths. The emission spectrum of the light source is shown on Figure 13. In the 'dark' or 'control' set the discs were kept in the dark at 37°C. Before irradiation the supernatant was removed from the wells and replaced with 0.2 ml phosphate buffer saline (PBS, PAA, United Kingdom) medium. After irradiation 10% 1 mg/ml MTT solution was added to the PBS solution. Following 4h incubation under standard conditions at 37°C the medium was gently removed from each well and the crystallized formazan dye was solubilized in absolute isopropanol supplemented with 0.04M HCl and 10% sodium dodecylsulfate. The optical density of the solution (OD_{540}) was determined at 540 nm with Organon Teknika Reader 530 (Organon Teknika, USA). Four (4) parallel experiments were performed including 4 samples per each experimental group as it is shown in Table 7 (151).

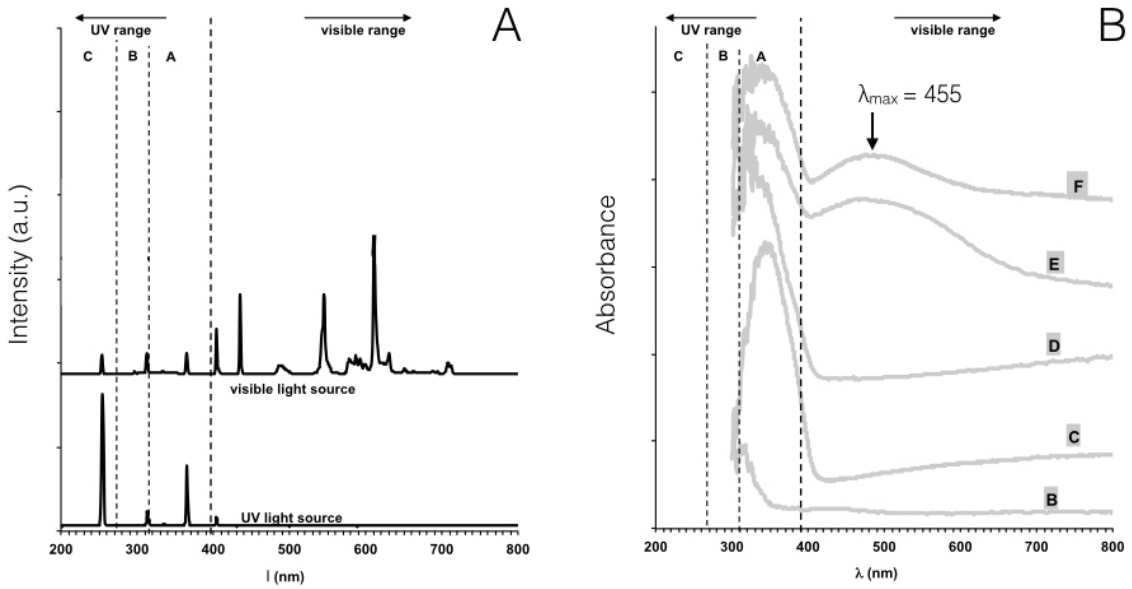

Figure 13. (a) Emission spectra of the UV-Vis light sources. The lower spectrum shows the emission lines of the UV light source that was used for the decomposition of p(EA-co-MMA) copolymer in the last step of the preparation of the samples. The upper spectrum shows the emission lines of both in the UV and VIS ranges of the light source that was used in the microbiology study for illumination. The low intensity emission lines can be observed at 254, 353 and 393 nm wavelengths. (b) UV-Vis absorption spectra of the experimental groups. The absorption spectra of the C-F experimental groups show large absorption band at 350 nm wavelength. Another absorption band appears on the absorption spectra of E-F groups in the VIS range between 400 and 550 nm with a maximum of 455 nm (151).

4.3.8 Statistical analyses

Quantitative results of the contact angle (CA, (°)), profile roughness of the surface (Ra, (μm)) and absorbance values (MTT, (1)) were analysed (151).

Data was grouped according to the applied surface treatment and whether the surface was irradiated or not. For data exploration, group means and their 95% confidence intervals were calculated using appropriate t-distributions centered at the sample mean of a given measurement group, with standard deviation equal to the standard error of the measurement within the group and degrees of freedom equal to the sample size in the group less one (151).

Absorbance values were further analysed to isolate the effects of the different surface treatments and the effect of irradiation on absorbance levels. Comparisons were made within treatment groups between irradiated and dark samples as well as across treatment groups. Due to the large number of comparisons and the highly different variances across groups a Bayesian multilevel linear model was used for the analysis. The following model was fit to the data in Stan and the output was analysed in Python (151, 163):

$$mtt_i = \alpha_{treatment[i]} + \beta_{treatment[i]} I_i + \epsilon_{treatment[i] \times irradiation[i]}$$

where

mtt_i is measured absorbance for the $i = 1 \ldots N$ (198) samples,

$\alpha_{treatment[i]}$ is the effect of surface treatment of the surface type present on sample *i*,

$\beta_{treatment[i]}$ is the effect of irradiation on the surface type of sample *i,*

I_i is the indicator variable showing if sample *i* was irradiated (1) or not (0),

$\epsilon_{treatment[i]}$ is the error term that is separately approximated for each surface type and irradiation condition.

The parameters were sampled the following way:

$\alpha_{1\ldots K} \sim \text{Normal}(T, \sigma_T)$ $\beta_{1\ldots K} \sim \text{Normal}(C, \sigma_C)$ $\epsilon_{1\ldots 2K} \sim Normal(0, \sigma_{E=1\ldots 2K})$

thus there are separate treatment, irradiation effects estimated for the *K*=6 (A-F) surface types and errors with different variances for the 2*K*=12 surface-irradiation combinations. The *T* (mean MTT absorbance for dark samples), *C* (mean effect of irradiation), σ_T, σ_C, σ_E scale hyperparameters are estimated from the data along with the $\alpha_{1\ldots K}$, $\beta_{1\ldots K}$ parameters of interest using Markov Chain Monte Carlo (MCMC) sampling in Stan. The hyperparameters were given minimally informative priors to constrain results to sensible ranges and aid sampler convergence. Sensitivity analysis was done to confirm priors(151).

The result of interest of the MCMC sampling is an empirical joint posterior distribution for the $\alpha_{1\ldots K}$, $\beta_{1\ldots K}$ parameters (mean surface treatment and irradiation effects), which allows direct comparison of the means as well as the actual measurements expected from future experiments. The probability distributions of the contrasts of the means as well as the predictive differences between individual measurements (containing data level variation) were calculated between and across treatment groups and irradiation conditions and were summarized by the 95% equal tailed probability intervals and

expected values of the distributions. These results are close to the values given by the t-distributions used in the data exploration; however, they are not necessarily equal due to the difference in the interpretation of a Bayesian credible interval and classical confidence intervals. We used the joint posterior distributions of the parameters to simulate comparisons of absorbance for individual samples and superimposed the resulting 95% CIs on the group means to indicate data level uncertainty. Data tables and plots were prepared using R (151, 164).

5 RESULTS

5.1 *In vitro* biocompatibility of prosthetic materials with human epithelial cells

5.1.1 Cell attachment and proliferation on prosthetic materials

After 24 hours, the mean percentage reduction of AB was 21.7 ± 2.8% for the Li-disilicate sample, 10.5 ± 3.0% for the zirconia samples and 12.3 ± 3.4% for the CoCr alloy sample. The highest cell attachment among the restorative materials was observed on Li-disilicate samples. Significant difference was found between attachment on zirconium-dioxide and Li-disilicate samples ($p < 0.045$ according to all post hoc tests). Li-disilicate showed the highest attachment (155).

After 72h the reduction was 40.9 ± 7.0% for the Li-disilicate sample, 25.2 ± 4.3% for the zirconia sample, and 29.1 ± 5.9% for the CoCr alloy sample. As in case of cell attachment, the epithelial cells proliferated better on the Li-disilicate samples. (155).

The comparison of the 24h (attachment) and 72h (proliferation) resulted in the following values: control plate: ($p = 0.001$), Li-disilicate: ($p = 0.011$), zirconia: ($p = 0.032$), CoCr: ($p = 0.015$) (155). Results are presented on Figure 14.

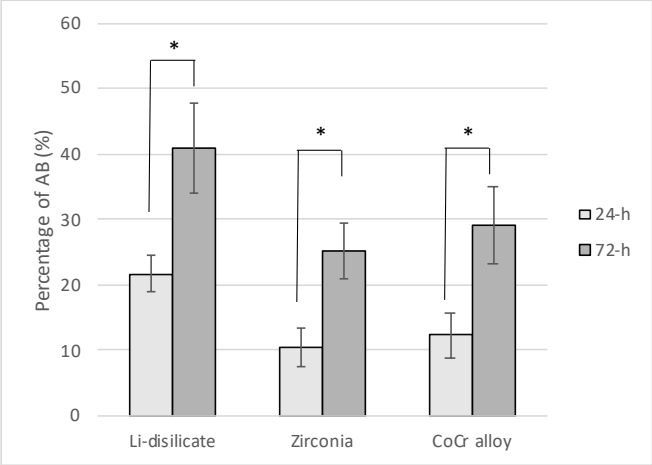

Figure 14 shows the 24-h and the 72-h percentage reduction of AlamarBlue (AB) on control cell culture plate, Li-disilicate, zirconia and CoCr alloy samples. Significant difference was found between the attachment (24-h observation) on Li-disilicate and zirconia samples ($p < 0.045$).

5.2 *In vitro* biocompatibility of laser ablated TiO_2 surfaces

5.2.1 Surface characteristics of the laser ablated TiO_2 surfaces

The results show that laser ablation significantly decrease the surface roughness of the sandblasted/acid etched samples (Figure 15 and 16). For the original sandblasted/acid etched samples the Ra value was 544 ± 47 nm (Figure 15A). As revealed by the AFM micrographs, for the frequency-doubled Q-switched Nd:YAG laser ablated samples (λ = 532 nm, 200 pulses, pulse energy = 40 mJ, FWHM = 10 ns, fluence = 1.3 J/cm2) Ra was 275 ± 36 nm (Figure 15B). For the samples irradiated with 2000 pulses of a KrF excimer laser (λ = 248 nm, pulse energy = 10 mJ, FWHM = 18 ns, fluence = 0.4 J/cm2) the Ra value was 288 ± 25 nm (Figure 15C). The bar graph of the AFM measurements is shown in Figure 16 (13).

The SEM images (Figure 17) revealed significant differences in the topography of the original (control) and the laser-irradiated TiO_2 surfaces. The control samples exhibit typical sandblasted/acid-etched surface structures (Figure 17A). On the Nd:YAG laser-ablated samples peculiar island-like crack areas appeared interrupted with point-holes. The average size of the 'islands' was ~15–20 µm (Figure 17B). In contrast, mainly rounded, almost uniform TiO_2 structures ~5–10 µm in diameter were observed on the excimer laser-treated samples (Figure 17C) (13).

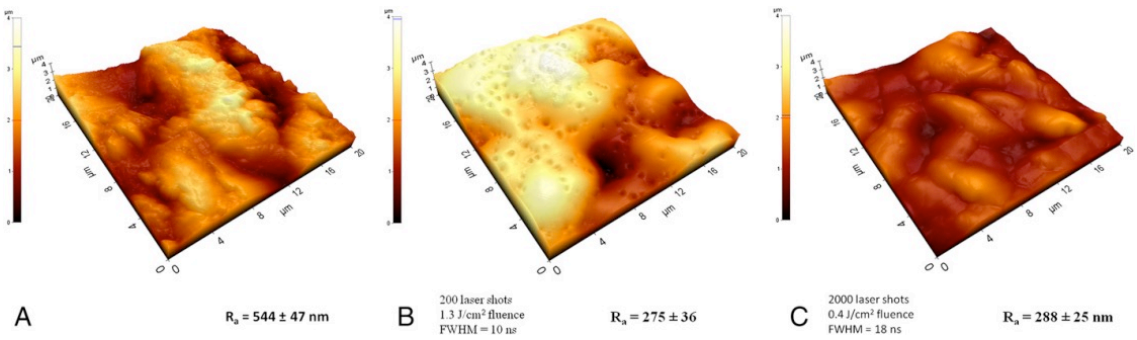

Figure 15 shows the AFM images of (A) a sandblasted/acid etched titanium surface (control), (B) a Nd:YAG laser-ablated surface and (C) a KrF excimer laser-ablated surface (151). The representative images show the decreased roughness of the laser ablated surfaces (B-C) in comparison to the starting surface (A) (referred to as control).

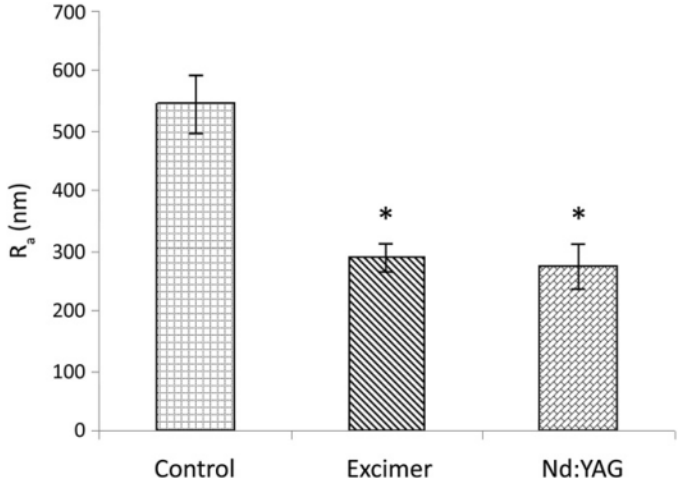

Figure 16 shows the bar graph of the AFM measurements. The results shows that the laser ablation significantly decreased the surface roughness irrespective to the applied laser type ($p < 0.05$) (151).

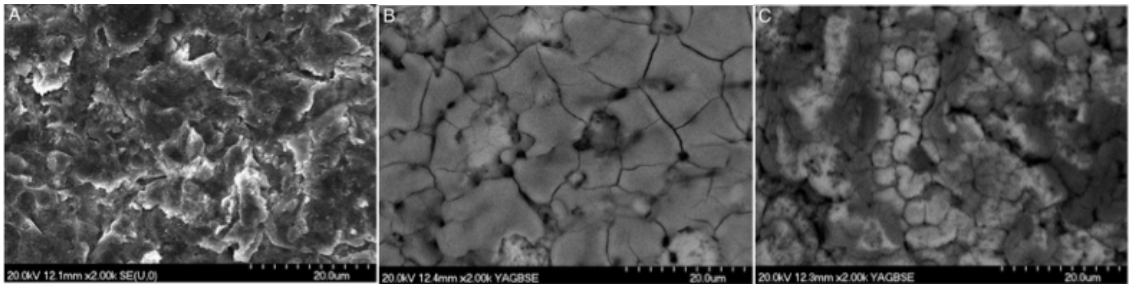

Figure 17 shows the SEM images of a sandblasted/acid-etched surface TiO_2 (control), a KrF excimer laser-ablated surface (2000 pulses, FWHM = 18 ns, fluence = 0.4 J/cm^2), and a Nd:YAG laser-ablated surface (200 laser shots at a fluence of 1.3 J/cm^2, FWHM =10 ns). The laser-ablation resulted in smoother surfaces (B-C) than the original (control) surface (A) (151).

5.2.2 Cell attachment investigated by SEM

Figure 18 (A, B, C) illustrates the SEM pictures of the attachment of the MG-63 osteoblast-like cells to different titanium surfaces after 24-h culturing. SEM did not reveal any morphological differences on the attachment and the growing of cells either on control or treated titanium surfaces. The cells exhibited spherical morphology (Figure 18B) typical for the attachment phase and signs of spreading behaviour were visible. On

the excimer laser treated Ti discs cells were more homogenously spread on the surface (13).

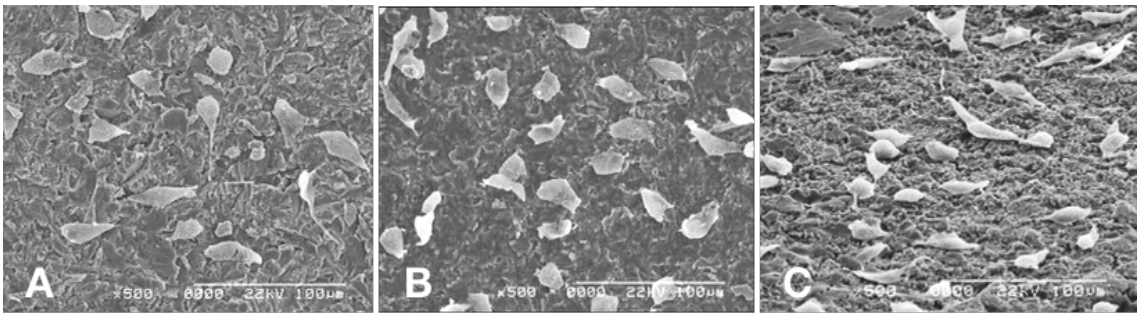

Figure 18. SEM images of MG-63 osteoblast-like cells attachment (24-h observation) on (A) an acid-etched and sand-blasted Ti surface (control), (B) a Nd:YAG laser-ablated Ti surface and (C) a KrF excimer laser-ablated Ti surface. Magnifications: 500x. SEM did not reveal any morphological differences on the attachment and the growing of cells either on control or treated titanium surfaces (13). Image (B) shows unpublished data.

5.2.3 Cell attachment and proliferation on laser ablated TiO_2 surfaces

5.2.3.1 MTT assay

The results of MTT measurements relating to cell attachment (24-h observation) and cell proliferation (72-h observation) are illustrated in the bar graphs of Figure 19. The mean ± $\sigma_{\bar{x}}$ of the OD_{540} values observed after 24-h observation were 0.246 ± 0.024 for the cells seeded on the plate itself, 0.150 ± 0.040 for the control sample, 0.153 ± 0.026 for the Nd:YAG laser-treated samples, and 0.146 ± 0.024 for the excimer laser-treated sample. No statistical differences were observed between the groups after the 24-h observation. The mean ± $\sigma_{\bar{x}}$ of the OD_{540} values observed after 72 h were 0.656 ± 0.037 on the plate, 0.410 ± 0.056 for the control sample, 0.403 ± 0.020 for the Nd:YAG laser-treated sample, and 0.372 ± 0.059 for the excimer laser-treated sample. The MTT data indicated that the MG-63 osteoblast-like cell proliferation on all the Ti surfaces was statistically significantly enhanced at 72-h relative to the cell attachment at 24-h ($p < 0.05$). No significant differences were observed between the groups after the 72-h proliferation (13).

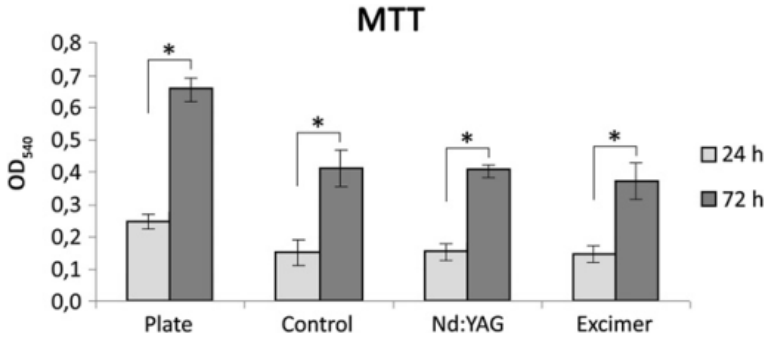

Figure 19 shows 24-h and 72-h percentage reduction of MTT on the plate, the control samples, the Nd:YAG laser-irradiated samples and the excimer laser-treated samples (13).

5.2.3.2 AlamarBlue assay

The percentage reduction was calculated from the OD_{570} and OD_{600} values for each well, as recommended in the protocol provided by the manufacturer (167). After 24 h, the mean percentage reduction of AB was 30.36% ± 4.15% on the plate, 18.95% ± 2.21% for the control sample, 19.80% ± 2.64% for the Nd:YAG laser-treated samples and 19.09% ± 2.06% for the excimer laser-treated sample. No statistical differences were observed between the groups after the 24-h observations. After 72 h the reduction was 59.20% ± 3.56% on the plate, 49.91% ± 3.29% for the control sample, 51.69% ± 3.83% for the Nd:YAG laser-treated sample, and 49.87% ± 3.22% for the excimer laser treated sample. The 72-h observations revealed statistically significantly enhanced cell proliferation on all the surfaces relative to the cell attachment ($p < 0.05$). No significant differences were observed between the groups after the 72-h proliferation. The results of AB measurements are illustrated in the bar graphs of Figure 20 (13).

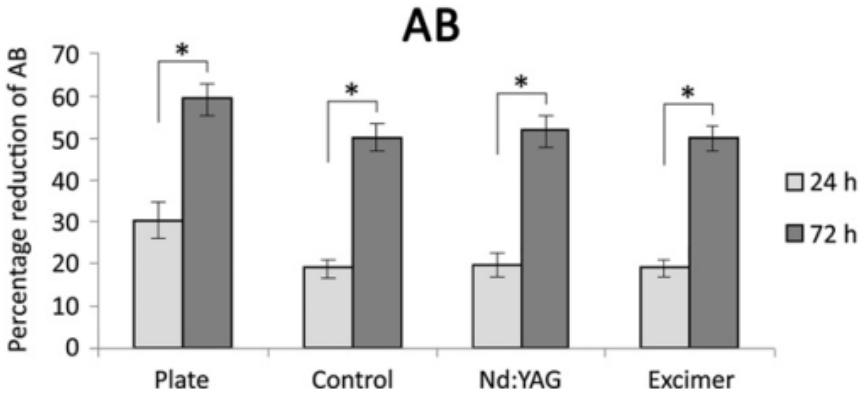

Figure 20. 24-h and 72-h percentage reduction of AB on the plate, the control samples, the Nd:YAG laser-irradiated samples and the excimer laser-treated samples (13).

5.2.4 Cell differentiation on laser ablated TiO_2 surfaces

The results of the differentiation tests are represented in Figure 21. The mean ± $\sigma\bar{x}$ of the OD_{504} values of the 3-day observation was 0.203 ± 0.002 for the control sample, 0.184 ± 0.003 for the Nd:YAG laser-treated samples, and 0.199 ± 0.004 for the excimer laser-treated sample. Statistically ($p < 0.05$) a decreased secretion of ALP was observed on the Nd:YAG surface treated samples compared to the control ones. The mean ± $\sigma\bar{x}$ of the OD_{504} values of the 7 day observations was 0.210 ± 0.002 for the control sample, 0.211 ± 0.003 for the Nd:YAG laser-treated sample, and 0.205 ± 0.002 for the excimer laser-treated sample. These data indicated that after 7 days of incubation, no statistical differences in the secretion of ALP were seen between the control and the laser-treated groups (13).

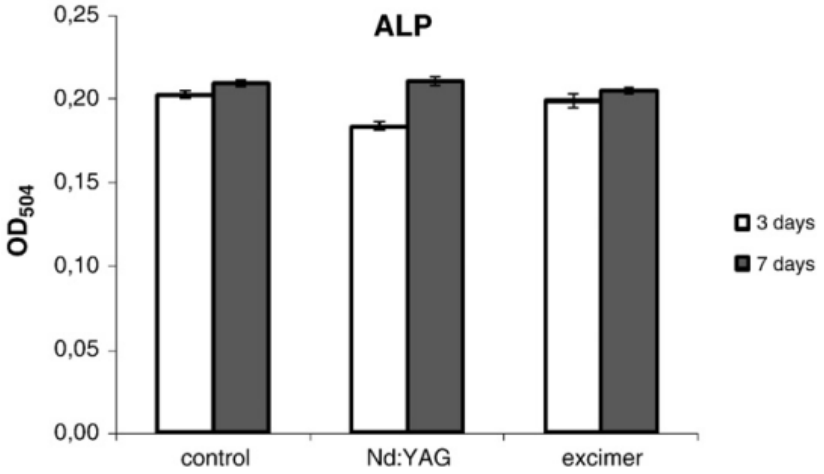

Figure 21. ALP activity (OD_{504}) after 3-days and 7 days observation on the control samples, the Nd:YAG laser-irradiated samples and the excimer laser-treated samples (13).

5.3 *In vitro* antibacterial property of nanocomposite polymers

5.3.1 Surface characterization of the Ag/TiO_2/polymer nanohybrid coatings

The SEM images revealed significant differences in the morphology of the intact and polymer coated TiO_2 surfaces at 500-fold magnification (Figure 22). Figure 22(a) shows a sandblasted/acid-etched TiO_2 surface that represents the typical surface pattern of a conventional titanium dental implant. Figure 22(b) shows a smooth surface that is obtained after acrylate-based copolymer film coating of the sandblasted/acid etched TiO_2 surface. Figure 22(c) and (d) shows the amorphous surface pattern in the micrometre range when the titanium discs were coated with a TiO_2 photocatalyst containing copolymer film; while characteristic rounded grains appeared on the surfaces of the discs that were coated with the silver photocatalyst containing copolymer film (Figure 22(e) and (f)) (151).

The quantitative measurement of roughness (Ra (mm)) on the surface of the discs by profilometry provided results that confirmed the differences in the surface pattern of the samples that were observed on the representative SEM images (Figure 22). There was considerable variation in the roughness values of the different surfaces; however, no significant difference could be observed between untreated and UVC-treated samples within the same surface treatments (151).

Before UVC irradiation contact angle (CA, (°)) measurements showed that the (A), (C), (D) and (F) surfaces were hydrophilic (CA≤90°), while (B) and (E) were hydrophobic. Photocatalyst containing surfaces (C, D, E and F) became superhydrophilic after UVC (254 nm) irradiation, while the polymer coated (B) remained hydrophobic. The mean contact angles for each treatment group and irradiation condition and their 95% CIs can be seen on the right panel of Figure 23 (151).

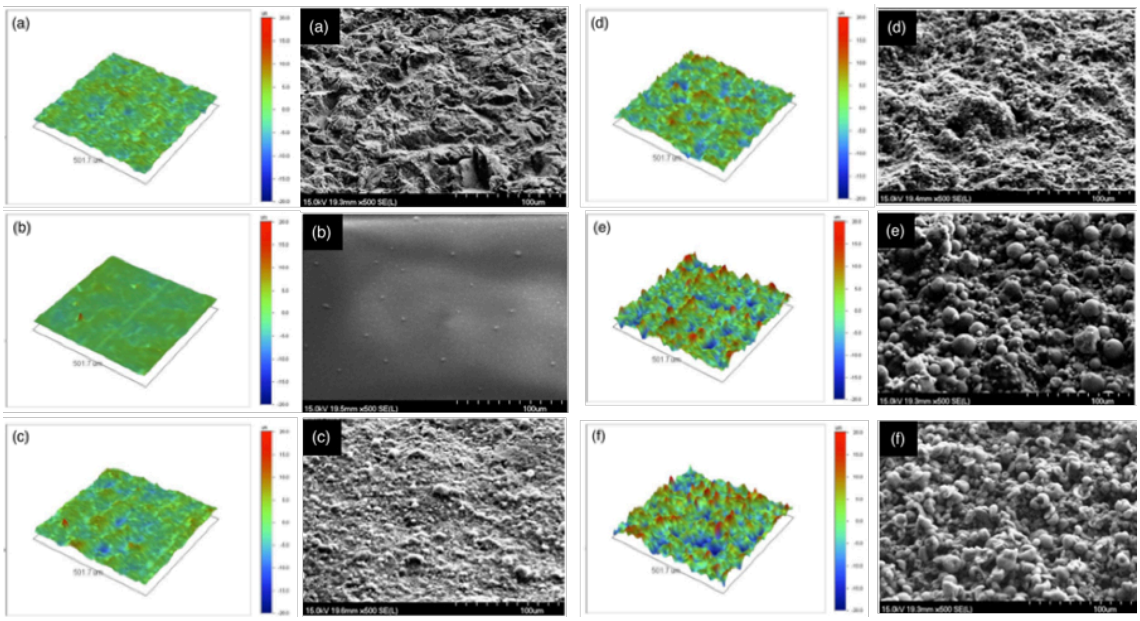

Figure 22 shows the representative SEM images and the three-dimensional roughness profiles of the surfaces. SEM images: (a) Sandblasted and acid etched surface (Group A), (b) p(EA-co-MMA) copolymer (Group B), (c) 60wt% TiO2 : 40 wt% copolymer (Group C), (d) 60 wt% DS-TiO2: 40wt% copolymer (Group D), (e) 60wt% Ag-TiO_2: 40 wt% polymer (Group E), (f) 60 wt% Ag-DS/TiO_2: 40 wt% copolymer (Group F). The average roughness values of the surfaces are the following: (a) Ra, A = 1.85 µm for sandblasted and acid etched surface (Group A), (b) Ra, B = 1.19 µm for p(EA-co-MMA) copolymer (Group B), (c) Ra, C = 2.33 µm for 60 wt% TiO_2 : 40wt% copolymer (Group C), (d) Ra, D = 3.70 µm for 60wt% DS TiO2 : 40wt% copolymer (Group D), (e) Ra, E = 5.17 µm for 60wt% Ag-TiO_2 : 40wt% copolymer (Group E), (f) Ra, F = 5.60 µm for 60wt% Ag-DS/TiO_2 : 40wt% copolymer (Group F) (151).

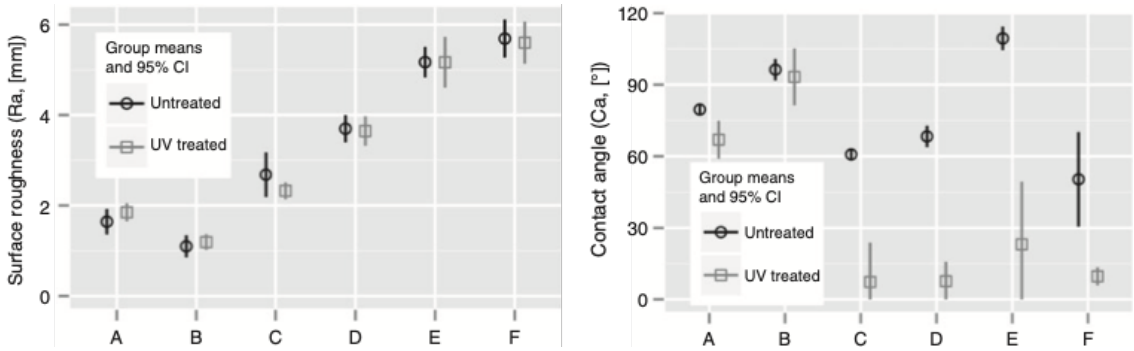

Figure 23 shows the surface roughness and contact angle values of the investigated surfaces. Means and 95% CIs of surface roughness and contact angles across surface types and irradiation conditions. There was considerable variation in surface roughness between the different surfaces; however, no significant difference could be observed between untreated and UVC-treated samples within the same surface treatments (top panel). Before UVC treatment contact angle (CA (º)) measurements showed that the (A), (C), (D) and (F) surfaces were hydrophilic, while (B) and (E) were hydrophobic. Photocatalyst containing surfaces (C, D, E and F) became superhydrophilic after UVC (254nm) treatment, while the polymer coated (B) remained hydrophobic. The mean contact angles for each treatment group before and after UVC treatment and their 95% CIs can be seen on the right panel.

5.3.2 Antibacterial property of the Ag/TiO_2/polymer nanohybrid coatings

Concerning the characterization of the clinical isolate of bacterium strain, the MALDI-TOF MS gave a species level identification with log(score)=2.184 for *S. salivarius* strain (151).

Absorbance levels (MTT, [1]) had distinct group means across most treatment and irradiation conditions as suggested by the minimal overlap in the confidence intervals (Figure 24). The linear decomposition of the absorbance levels into surface effects, surface-based irradiation effects and noise yielded comparative results. Under dark conditions, the group means of absorbance in the TiO_2 photocatalyst containing (C) and (D) experimental groups was higher than those of the Ag/TiO_2/polymer nanohybrid films in the (E) and (F) groups. This suggests that more *S. salivarius* attached to the surface of TiO_2 containing polymer films than to Ag/TiO_2/polymer nanohybrid films. The mean absorbance in the (E) and (F) groups was credibly lower than in any of the other groups. The control (A) group had the highest mean absorbance of all groups, being credibly higher than (B) and (D), but compared to group (C) a zero difference still falls in the 95% credible interval (151).

The net effect of UV-VIS irradiation on absorbance values was negative in each group (95% CI excluded zero), indicating that the viability of bacteria was reduced on the irradiated surfaces. The same tendency was observed on the control surface (A) after irradiation than in C, D and E, F experimental groups. However, this reduction was the lowest in the (B) experimental group where the control surface was coated with p(EA-co-MMA) polymer without any photocatalyst content. In absolute magnitude the highest irradiation effect of -0.15 $CI_{95\%}$(0.09, 0.21) was observed in the (C) group, while relative to the dark levels the (E) group showed the largest percentage change of 60% $CI_{95\%}$(50%, 67%), followed by group (C) 33% $CI_{95\%}$(23%, 42%). The credible differences are listed in Table 8-9 across comparisons both in the group means and the individual measurements, as well as an estimation of the percentage of the samples that we expect to have lower/higher absorbance in the comparison (Figure 25, Table 10) (151).

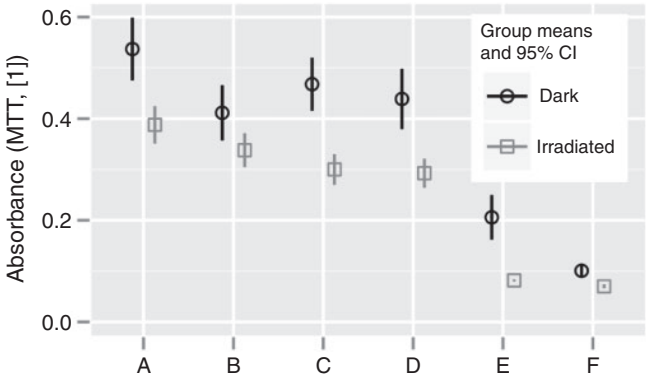

Figure 24 shows the mean MTT absorbance values are shown before and after UV-Vis irradiation. The lack of overlap suggests significant differences between certain groups; however, due to the apparent differences in variances, a Bayesian analysis was used to confirm this (151).

Table 8 shows the credible intervals for the difference in absorbance levels of the dark and UV-VIS irradiated experimental groups within the same surface types. A black typeface is used where the credible interval excludes zero, gray where the interval overlaps zero. Intervals for the mean difference and for individual differences are given, as well as an estimation of the percent of the samples that will have lower/higher absorbance in a one-to-one comparison (151).

	95% CI for mean difference in MTT absorbance			95% CI for individual differences in absorbance			Predicted % of diffs. being positive/negative	
Comparison	Low	Mean	High	Low	Mean	High	(+)	(-)
Ad - Al	0.07	0.13	0.20	-0.18	0.13	0.44	81%	19%
Bd - Bl	0.02	0.08	0.14	-0.19	0.08	0.36	73%	27%
Cd - Cl	0.09	0.15	0.21	-0.12	0.15	0.41	87%	13%
Dd - Dl	0.08	0.13	0.19	-0.15	0.13	0.42	83%	17%
Ed - El	0.08	0.12	0.17	-0.07	0.12	0.31	90%	10%
Fd - Fl	0.02	0.03	0.04	-0.02	0.03	0.08	89%	11%

Table 9 shows the credible intervals for the difference in absorbance levels of each surface type when kept in the dark. A black typeface is used where the credible interval excludes zero, gray where the interval overlaps zero. Intervals for the mean difference and also for individual differences are given, as well as an estimation of the percent of the samples that will have lower/higher absorbance in a one-to-one comparison (151).

	95% CI for mean difference in MTT absorbance			95% CI for individual differences in absorbance			Predicted % of diffs. being positive/ negative	
Compa-rison	Low	Mean	High	Low	Mean	High	(+)	(-)
Ad - Bd	0.03	0.11	0.18	-0.25	0.11	0.46	73%	27%
Ad - Cd	-0.01	0.07	0.15	-0.28	0.07	0.43	66%	34%
Ad - Dd	0.02	0.10	0.17	-0.28	0.10	0.47	70%	30%
Ad - Ed	0.25	0.32	0.39	-0.01	0.32	0.65	97%	3%
Ad - Fd	0.36	0.42	0.48	0.14	0.42	0.70	100 %	0%
Bd - Cd	-0.11	-0.04	0.03	-0.36	-0.04	0.29	41%	59%
Bd - Dd	-0.08	-0.01	0.06	-0.36	-0.01	0.34	47%	53%
Bd - Ed	0.15	0.21	0.28	-0.09	0.21	0.52	92%	8%
Bd - Fd	0.26	0.32	0.37	0.07	0.31	0.56	99%	1%
Cd - Dd	-0.05	0.03	0.10	-0.32	0.03	0.37	56%	44%
Cd - Ed	0.18	0.25	0.31	-0.05	0.25	0.55	95%	5%
Cd - Fd	0.30	0.35	0.40	0.11	0.35	0.59	100 %	0%
Dd - Ed	0.16	0.22	0.29	-0.10	0.22	0.54	92%	8%
Dd - Fd	0.27	0.33	0.38	0.06	0.33	0.59	99%	1%
Ed - Fd	0.06	0.10	0.15	-0.10	0.10	0.30	85%	15%

Table 10 shows the credible intervals for the difference in absorbance levels of each surface type after UV-VIS irradiation. A black typeface is used where the credible interval excludes zero, gray where the interval overlaps zero. Intervals for the mean difference and for individual differences are given, as well as an estimation of the percent of the samples that will have lower/higher absorbance in a one-to-one comparison (151).

	95% CI for mean difference in MTT absorbance			95% CI for individual differences in absorbance			Predicted % of diffs. being positive/negative	
Comparison	Low	Mean	High	Low	Mean	High	(+)	(-)
Al – Bl	0.01	006	0.10	-0.16	0.06	0,27	70%	30%
Al – Cl	0.04	0.09	0.14	-0.12	0.09	0,29	81%	19%
Al – Dl	0.05	0.10	0.14	-0.10	0.10	0.30	84%	16%
Al – El	0.27	0.31	0.35	0.15	0.31	0.47	100%	0%
Al – Fl	0.29	0.32	0.36	0.16	0.32	0.48	100%	0%
Bl – Cl	-0.01	0.03	0.08	-0.16	0.03	0.23	63%	37%
Bl – Dl	0.00	0.04	0.08	-0.15	0.04	0.23	68%	32%
Bl – El	0.22	0.25	0.29	0.11	0.25	0.40	100%	0%
Bl – Fl	0.23	0.27	0.30	0.12	0.27	0.41	100%	0%
Cl – Dl	-0.03	0.01	0.05	-0.17	0.01	0.19	54%	46%
Cl – El	0.19	0.22	0.25	0.09	0.22	0.35	100%	0%
Cl – Fl	0.20	0.23	0.27	0.10	0.23	0.37	100%	0%
Dl – El	0.18	0.21	0.24	0.09	0.21	0.34	100%	0%
Dl – Fl	0.20	0.22	0.25	0.10	0.22	0.35	100%	0%
El – Fl	0.01	0.01	0.02	-0.01	0.01	0.03	88%	12%

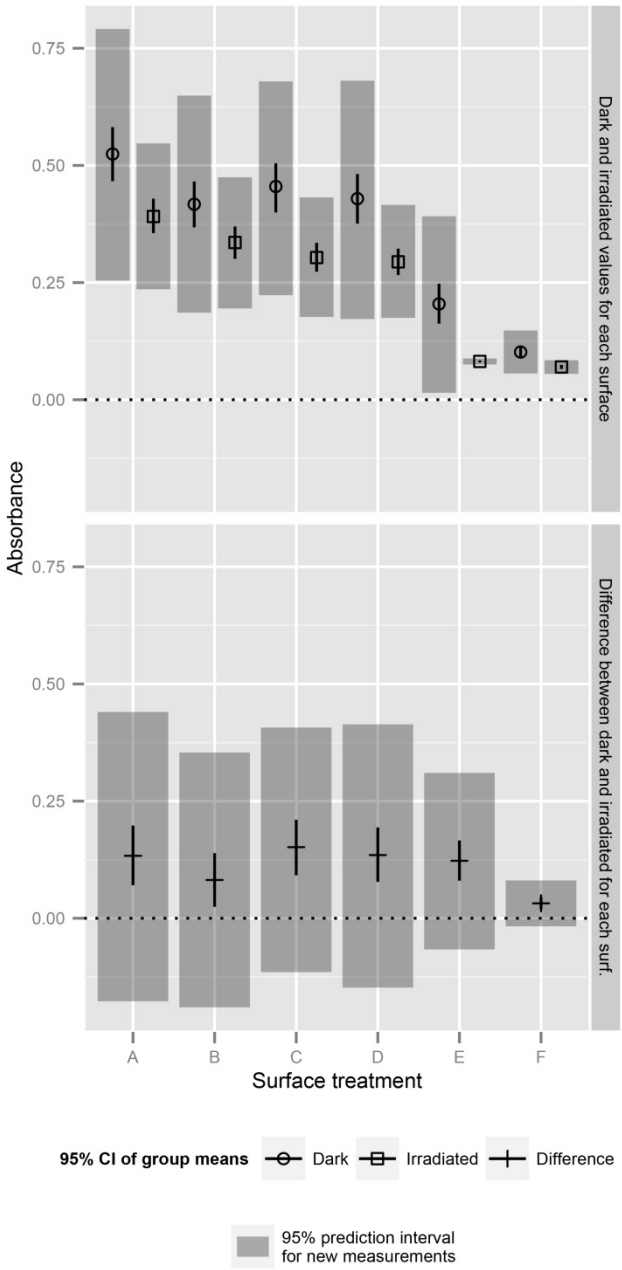

Figure 25 shows the credible intervals of absorbance across surface types and irradiation conditions and credible differences between irradiated and dark samples within the same surface types. 95% CIs of group means, and individual measurements are displayed. Under dark conditions, the group means of absorbance in the TiO_2 photocatalyst containing (C) and (D) experimental groups was higher than those of the coupled Ag/TiO_2 containing films in the (E) and (F) groups. The mean absorbance in the (E) and (F) groups was credibly lower than in any of the other groups. The control (A) group had the highest mean absorbance of all groups, being credibly higher than (B) and (D) but compared to group (C) a zero difference still falls in the 95% credible interval (151).

6 DISCUSSION

Our results showed that restorative materials had good *in vitro* biocompatibility with oral mucosa derived epithelial cells. Laser ablation did not improve the biocompatibility of TiO_2 surfaces with MG-63 cells compared to the control sandblasted/acid-etched surfaces. Credible correlation between the physical and physicochemical properties of the polymer surfaces, i.e. between roughness and wettability, and the antibacterial property could not be established, however the effect of the composition of polymers was obvious. TiO_2 and silver coupled TiO_2 containing nanocomposite polymers showed significant photocatalytic antibacterial property after UV-VIS irradiation. Silver coupled TiO_2 nanocomposite polymer showed contact *in vitro* antibacterial property without irradiation. Surprisingly, the control sandblasted/acid-etched TiO_2 surfaces showed some UV-VIS irradiation induced antibacterial property, too.

The first critical period concerning the survival of dental implants is the first week after the implantation when the gap-free closure of gingiva should develop around the neck of the implant and prosthetic abutment. The good biocompatibility of the prosthetic and implant materials with epithelial cells is the prerequisite of the fast development of the biological barrier that excludes the bacteria of oral flora from the wound. If this process is impaired for any reason it may prolong the wound healing and increase the risk of the development of primary peri-implantitis. Our results suggest that the currently applied prosthetic materials support the development and maintenance of gap-free biological sealing. Hence, it may not be the low biocompatibility of these prosthetic materials in the background of primary peri-implantitis, but other causatives. To reveal the etiology of primary peri-implantitis requires further research that is beyond the scope of the present doctoral work.

Based on data available in the literature we expected that laser ablation was going to further increase the roughness of the sandblasted/acid-etched TiO_2 surfaces, but surprisingly the opposite happened, it smoothed the surfaces. The high surface roughness is supposed to improve the osseointegration of the titanium implants, albeit our results do not show any difference in the *in vitro* biocompatibility between the sandblasted/acid-etched and laser ablated TiO_2 surfaces. This finding is not surprising in the light of

discrepancies in the available data in the literature concerning the correlation between surface roughness and biocompatibility.

Surface roughness has been in the focus of research and development for decades and many authors have recommended roughness ranges that have been believed to enhance the biological and clinical performance of titanium dental implants. These recommendations may be biased though, because they are often based on publications with shared conviction that perceive surface roughness as the paramount design feature of dental implants. Contrarily, there are several publications that claim the superiority of smooth TiO_2 surfaces against rough ones. These arguments are based on pre-clinical studies that are not confirmed with clinical data. It is almost impossible to find clinical studies that compare different surface properties with the same geometry and host conditions. This sort of standardization of the experimental design of clinical studies would be necessary to exclude other factors that may have a significant influence on the clinical outcome and allow drawing sound conclusions concerning the effect of surface roughness. Only a few studies can be found that investigate the effect of a single parameter on the implant at once. This fact questions the credibility and soundness of any conclusion and recommendation on the putative optimal level of surface roughness in conjunction with titanium dental implants.

For instance, Straumann's SLActive surface is one of the most often cited brand in the literature suggesting the superiority of this surface. The SLActive surface is acid-etched and subsequently sandblasted that is rinsed and packed in isotonic saline under inert N_2 atmosphere. In contrast, SLA surface, an earlier design of SLActive, is produced according to the same method, but instead of protective N_2 atmosphere, the implant is packed in a clean room under germ-free air. Pre-clinical results show that the osseointegration of SLActive surfaces is faster than that of SLA surfaces in the early phase (165). This advantage is attributed to the extreme hydrophilicity of the SLAactive surface that enhances the primary contact with the body fluids. However, we cannot find data demonstrating the superiority of the SLAactive in clinical settings, implying primary and secondary stability of this sort of implants (116).

Immediate loading of dental implants is a recent trend and some branded implant surfaces, such as Laser Lok claims this indication in its marketing materials. However,

there is not available clinical data that support the survival of immediately loaded implants over 5 years. Based on the argument above it can be stated that there are some particular surfaces that show better histomorphometric results in early osseointegration in preclinical studies, but these results are not supported with sufficient clinical data (116).

Concerning the surface of titanium dental implants, the only fact that is supported with objective evidence is that the TiO_2 layer is responsible for the biocompatibility, which was discovered by Branemark in the 60's. His very first titanium implant had a moderately smooth machined surface that is also referred to as turned surface in the literature (166). Titanium implants with machined surfaces were in clinical use for the 90's and they showed excellent osseointegration. Albrektsson *et al.* recommended first the roughening of the surface of titanium dental implants, which created an overwhelming demand for rough surfaces. Indeed, the need for rough surfaces has become a creed in implantology superseding machined surfaces completely (6). Although, Albrektsson recommended moderate surface roughness, but it has become a general belief that the rougher the surface is the better the osseointegration. There are long-term studies that prove the clinical equivalence of machined and rough titanium implant surfaces; thus, the superiority of the latter may not be credibly claimed (167). In *in vitro* experiments it has been verified by various researcher groups that the properties of the implant surface have influence on the adherence, proliferation and differentiation of osteogenic cells, however the role of surface roughness in the long-term survival of the implants is not supported with sufficient clinical data (168).

It also can be stated that there is no evidence for the beneficial effect of any kind of surface treatment on the osseointegration and survival of dental implants. In contrast, it has been clearly proven based on both pre-clinical and clinical data that rough TiO_2 surfaces facilitate the adherence of pathogenic bacteria, the development of peri-implantitis and reduce the treatment efficacy of biofilms (169-171).

According to the 'race for the surface' theory when a biomaterial is inserted in the bone the healing process begins that results in the colonization of osteogenic cells and tissue formation (172). If bacteria reach the surface first, then they will have room for colonization displacing stromal cells from the surface of the implant. In principle, the

success of the integration of a biomaterial depends on the outcome of this race between bacteria and stromal cells. In the course of implant surgery, the dental implants are taken out from a sterile package and conveyed to the surgical site through the non-sterile ambient air of the operating room, and certainly will get in contact with the mucosal tissue, saliva, blood, and the bone tissue. During that time, the chance for bacterial contamination of the implant surface is very high. Thus, it is presumable that some bacteria adhere to the surface of the implant in the course of the invasive surgical intervention that is carried out in the non-sterile environment of the oral cavity. Even if osseointegration takes place without disturbance these bacteria may remain dormant on the surface of the implant for years, but they may turn metabolically active when the physiological conditions become favorable for them, for instance, if local inflammation occurs (173).

Even if the enhanced biocompatibility of rough TiO_2 surfaces is not proven unambiguously, but they are supposed to support the secondary stability of the implants after osseointegration; therefore, rough implant surfaces, even if they are more susceptible for bacterial infections will prevail presumably. This prompted our aspiration to attempt the development of a surface treatment method that may be suitable to prevent the peri-implant infections of titanium dental implants in the long-run. The electronic properties of silver coupled TiO_2 nanoparticles have been successfully utilized to enhance the performance of solar cells, and we tried to take the advantage of the same mechanism in the creation of antibacterial surfaces (174).

Silver is known as a broad-spectrum antibacterial agent, a component of various pharmaceutical products, albeit its use in association with medical devices has been limited due to its putative cytotoxic property (175, 176). On the other hand, the spreading antibiotic resistance of bacteria calls for alternative technologies that can prevent bacterial infections without contributing to the further development of their resistance.

The spreading antibiotic resistance among bacteria has become one of the leading challenges of life sciences. The root cause has been the overuse of antibiotics in the last few decades, which tendency does not seem to subside even nowadays. Concerning dentistry and oral surgery, still, lots of antibiotics are used for prevention and aftercare. According to a Spanish cross-sectional study, 88% of the dentists order prophylactic

antibiotic cure routinely before implant surgery, while only 9% of the doctors consider other circumstances (177). They do all this even though there is currently no clear guideline about the need for prophylactic antibiotic. In their meta-analysis, Lund *et al*. could not prove the necessity of prophylactic antibiotic use in routine, uncomplicated cases (178). Of course, there are complicated cases when antibiotic prophylaxis is justified, but the uncontrolled use of antibiotics contributes to the increasing resistance of bacteria. Antibiotics are also used in the conservative treatment of peri-implant infections, though they are useful only for symptomatic treatment, they cannot eliminate the bacteria from the surface of the implant (179). Thus, based on the currently available evidence, the use of antibiotics without due care will only contribute to the further strengthening of the resistance of bacteria. There may be a greater need for breakthrough innovations in this domain than any time before because pharmaceutical companies do not invest in the research and development of new antibiotics anymore. The European Commission has recognized this problem and made significant efforts to boost innovation, especially the development of alternative antibacterial technologies.

Based on the available *in vitro* data in the literature, the toxicity of silver nanoparticles is mainly associated with their cellular uptake where they trigger intracellular oxidative stress leading to cell death (139). Our surfaces contain immobilized AgNP that does not allow the release and uptake of the nanoparticles. Our results show that the immobilized AgNP retained their bactericidal capability even without photon-induction (in the dark), but the mechanism of action was not investigated in our studies. However, it is important to understand the underlying biochemical processes to be able to objectively consider the associated clinical risks. The findings of other researcher groups suggest that there may be at least two mechanisms that should be taken into consideration. One possible mechanism of action could be attributed to the capability of AgNPs to displace cations (K^+ and Ca^{2+}) from the bacterial cell envelop causing the separation of the cell wall from the cytoplasmic membrane both in Gram-positive and Gram-negative bacteria. But, because the AgNPs are immobilized on our surfaces, only partial displacement of cations may be assumed that might not be sufficient alone to trigger cell death. Another possible mechanism is that the dissolution of silver ions from the surface of the AgNPs might have a synergistic effect on the displacement of the nanoparticles (180). The antibacterial mode of action of silver ions is connected to

the destabilization of the bacterial envelope, interaction with intracellular molecules and the production of ROS (181).

Other members of our research team showed in their study that MG63 cells and primary epithelial cells can attach and proliferate on the surface of Ag-TiO_2 nanocomposite polymer. However, it must be noted that the concentration of the Ag nanoparticles needed to be reduced from 0.5 w/t% to 0.01 w/t % in order not to kill the cells (184).

From a clinical perspective, it is a critical question of how long the structure and composition of the coating can retain its antibacterial capability. Concerning Ag coupled TiO_2 nanoparticles, it is presumable that silver ions will dissolve from the surface of the metallic nanoparticles. The driving force of the dissolution is not galvanic corrosion (TiO_2 does not obey the rules of galvanic corrosion) but thermodynamics. The rate of dissolution and the concentration of the released silver ions in the body influence the benefit-risk profile of these sort of surfaces. Thus, the control of the kinetics of the silver dissolution is pivotal to achieve the intended performance of the Ag coupled TiO_2 surface.

The second critical period concerning the survival of dental implants comes after 5 years of the osseointegration of the implant, usually when secondary peri-implantitis develops due to the inappropriate loading of the implant. It would take long-term follow-up studies to fully establish the safety profile of implant surfaces with Ag coupled TiO_2 nanoparticles, but we suppose that the exposition of the surrounding tissues to silver ions for the entire lifetime of the implant might cause unforeseeable side-effects. The risk of adverse events might be mitigated by the design and technical features of the surface. Concerning Ag coupled TiO_2 nanoparticles, the Ag nanoparticles should be designed to deplete within a reasonable time, for instance, after the risk of primary peri-implantitis is considered reasonably low.

The UV-VIS induced antibacterial property of the Ag coupled TiO_2 and bare TiO_2 nanoparticle containing polymers may open a new opportunity for the conservative treatment of peri-implant infections that is more efficient than the currently available medical alternatives. For instance, if primary peri-implantitis develops the complete removal of bacteria from the implant surface might be achievable by the illumination of

the Ag coupled TiO_2 nanoparticles with an ordinary dental curing lamp having emission in the UV-VIS ranges that is easily accessible within 1-3 weeks after the implant surgery. The intense photon-induced release of ROS from the implant surface in the close vicinity of the adhered bacteria may be more effective than surgical decontamination because it does not impair the surface. Since the bare TiO_2 containing polymer also showed considerable UV-VIS induced antibacterial property, the same mechanism may be utilized in treatment of secondary peri-implantitis, when silver is already depleted from the surface. The ultimate therapeutic goal is the complete removal of bacteria from the surgical site, implying the implant surface and the surrounding tissues. The surrounding tissues can be decontaminated by surgical debridement, but there is no effective method to eliminate the bacteria from the implant surface. The currently applied surgical decontamination of the implant surfaces does not guaranty the complete elimination of bacteria but causes irreversible damage to the surface deteriorating its ability for the osseointegration. The proposed nanocomposite polymers may offer an alternative solution for this problem.

The results of this thesis should be interpreted in light of its limitations. The antibacterial property of our surfaces was tested on one early colonizer bacterium strain, only. The medical application of the poly(ethyl acrylate-co-methyl) methacrylate resin is not known, implying biocompatibility and the risk that nanoparticles may release from the polymer if its resistance to enzymatic degradation is insufficient. There is limited data available on the cytotoxicity of AgNPs, however, the findings of other authors suggest that they seemingly cause less damage to eukaryotic cells than silver ions *in vitro* (182, 183). Other authors argue that the cytotoxicity of AgNPs depends not exclusively on concentration, but the geometry and manufacturing method of the nanoparticles, as well. Hence, it is difficult to judge the cytotoxicity, but even more the clinical safety of AgNPs in general. The drop in the absorbance level after the illumination of the control surfaces with UV-VIS light source may not be explained based on the antibacterial mechanisms detailed in the body of the thesis.

7 CONCLUSIONS

7.1 Prosthetic materials show good *in vitro* biocompatibility with human mucosa derived epithelial cells; they might be suitable to support the prevention of primary peri-implantitis.

7.2 Laser ablated TiO_2 surfaces do not show superior *in vitro* biocompatibility compared to the conventional SLA surfaces; they might not be suitable to support the prevention of secondary peri-implantitis by the enhancement of the secondary implant stability.

7.3 Silver and TiO_2 embedded nanocomposite polymers show good photo-induced *in vitro* antibacterial property on the surface of titanium samples; they might become promising candidates to support the prevention of the development of secondary peri-implantitis.

8 SUMMARY

One of the leading causes of the failure of titanium dental implants is related to implant-associated bacterial infections (peri-implantitis). Since the current medical technologies are not efficient in the curative treatment of peri-implantitis the prevention of the infections provides a plausible alternative strategy. One strategic approach has been the improvement of the biocompatibility of dental implants ensuring complete biological sealing around the implant in order to exclude pathogenic bacteria from the implant site. A more recent approach is the enhancement of the antibacterial feature of the surface of dental implants with the view to create an 'active' line of defence against bacterial infections. In my doctoral work I investigated the practical aspects of these two strategic approaches in *in vitro* experiments.

In the clinical practice it has been a widely-accepted perception that the appropriate biological sealing requires the gap-free adherence of the gingiva to the surface of prosthetic materials. However, the biocompatibility of these materials with human mucosa derived epithelial cells has not been known up to now. The stability of the implants can be improved by the enhancement of surface roughness, for which purpose lasers are used increasingly. I investigated the biocompatibility of laser ablated titanium surfaces and attempted to interpret the results in the context of the prevention of peri-implantitis. Concerning the improvement of the antibacterial feature of the titanium samples, the attachment and proliferation of *S. Salivarius* was investigated on the surface of titanium-dioxide (TiO_2) and silver containing nanocomposite coatings.

The epithelial cells attached and survived on the surface of the most often used prosthetic materials which suggests their suitability in the support of the complete biological sealing. Unlike expectations, the laser ablation reduced the surface roughness and did not improve the biocompatibility of the titanium samples, thus such surfaces may not be more efficient in the support of the biological sealing than the conventional surfaces. The sliver containing coatings significantly decreased the quantity of the bacteria on the surface in dark, while the nano-TiO_2 comprising coating showed significant antibacterial property under UV-VIS irradiation which raises the possibility of their application both in the prevention and treatment of peri-implantitis.

ÖSSZEFOGLALÁS

Napjainkban a fogászati titán implantátumok elvesztésének egyik vezető oka a bakteriális fertőzés eredetű peri-implantáris gyulladások kialakulása. A terápiás lehetőségek nem elég hatásosak a fertőzéseket gyógyításához, ezért jelenleg az elsődleges célunk a megelőzés lehet. Az egyik ilyen lehetőség a megfelelő biológiai záródás elősegítése az implantátum felépítménye körül, azaz kvázi elzárjuk az implantátum felületét a baktériumok elől. A másik lehetőség az implantátumok felületének antibakteriális tulajdonságainak javítása, amely így aktív védvonalat képez a bakteriális fertőzésekkel szemben. A doktori munkám során ennek a két megközelítésnek a gyakorlati vonatkozásait vizsgáltam *in vitro* kísérletekben.

A klinikai gyakorlatban elterjedt az a vélekedés, miszerint a biológiai záródás akkor a legmegfelelőbb, ha a nyálkahártya meg tud tapadni a felépítményen is, ezzel egy elsődleges védvonalat biztosítva a baktériumok behatolásával szemben. Ennek ellenére korábban nem volt ismert, hogy a felépítményekhez használt anyagokon milyen mértékben tudnak kitapadni és túlélni a humán nyálkahártya eredetű epitél sejtek. Az implantátumok stabilitása növelhető a felület érdességének növelésével, amiben a lézerek újabban egyre nagyobb teret nyernek. Megvizsgáltam a lézerkezelt titán felületek biokompatibilitását és megkíséreltem az eredményeket a peri-implantáris fertőzések megelőzésének kontextusában értelmezni. Az implantátumok antibakteriális tulajdonságának javítására vonatkozóan *S. Salivarius* megtapadását és túlélését vizsgáltam titán-dioxid és ezüst tartalmú nano-kompozit bevonatokon.

A felépítményként leggyakrabban használt anyagokon megtapadtak és szaporodtak a sejtek, ami azt sugallja, hogy azok megfelelőek a biológiai záródás elősegítésére. A várakozásokkal szemben a lézerkezelés csökkentette a titán minták érdességét és nem javította azok biokompatibilitását, vagyis vélhetően nem javítja a sejtek kitapadásának és szaporodásának gyorsaságát. Az ezüst tartalmú bevonatok sötétben is jelentősen csökkentették a baktériumok mennyiségét a felületen, míg a nano-titán tartalmú bevonat UV-VIS megvilágítás hatására mutatott jelentős antibakteriális hatékonyságot, ami felveti a bevonatok klinikai alkalmazhatóságának lehetőségét a peri-implantáris fertőzések megelőzésében és kezelésében is.

9 REFERENCES

1. Heydecke G, Locker D, Awad MA, Lund JP, Feine JS. (2003) Oral and general health-related quality of life with conventional and implant dentures. Community Dent Oral Epidemiol, 31(3): 161-168.
2. Awad MA, Locker D, Korner-Bitensky N, Feine JS. (2000) Measuring the effect of intra-oral implant rehabilitation on health-related quality of life in a randomized controlled clinical trial. J Dent Res, 79(9): 1659-1663.
3. Chug A, Shukla S, Mahesh L, Jadwani S. Osseointegration - Molecular events at the bone–implant interface: A review. (2013) J Oral Maxillofac Surg Med Pathol, 25(1): 1-4.
4. Branemark PI. (1983) Osseointegration and its experimental background. J Prosthet Dent, 50(3): 399-410.
5. Coelho PG, Jimbo R, Tovar N, Bonfante EA. (2015) Osseointegration: hierarchical designing encompassing the macrometer, micrometer, and nanometer length scales. Dent Mater, 31(1): 37-52.
6. Albrektsson T, Wennerberg A. (2004) Oral implant surfaces: Part 1- review focusing on topographic and chemical properties of different surfaces and in vivo responses to them. Int J Prosthodont, 17(5): 536-543.
7. Dohan Ehrenfest DM, Coelho PG, Kang BS, Sul YT, Albrektsson T. (2010) Classification of osseointegrated implant surfaces: materials, chemistry and topography. Trends Biotechnol, 28(4): 198-206.
8. Rasouli R, Barhoum A, Uludag H. (2018) A review of nanostructured surfaces and materials for dental implants: surface coating, patterning and functionalization for improved performance. Biomater Sci, 6(6): 1312-1338.
9. Kansas Dental Center (2019) Available from: http://www.ksdentalcenter.com/dental-implant/.

10. Adell R, Lekholm U, Rockler B, Branemark PI. (1981) A 15-year study of osseointegrated implants in the treatment of the edentulous jaw. Int J Oral Surg, 10(6): 387-416.
11. Branemark PI, Adell R, Albrektsson T, Lekholm U, Lundkvist S, Rockler B. (1983) Osseointegrated titanium fixtures in the treatment of edentulousness. Biomaterials, 4(1): 25-28.
12. Davies JE. (1998) Mechanisms of endosseous integration. Int J Prosthodont, 11(5): 391-401.
13. Gyorgyey A, Ungvari K, Kecskemeti G, Kopniczky J, Hopp B, Oszko A, Pelsöczi I, Rakonczay Z, Nagy K, Turzó K. (2013) Attachment and proliferation of human osteoblast-like cells (MG-63) on laser-ablated titanium implant material. Mater Sci Eng C Mater Biol Appl, 33(7): 4251-4259.
14. Ozkurt Z, Kazazoglu E. Zirconia dental implants: a literature review. (2011) J Oral Implantol, 37(3): 367-376.
15. Apratim A, Eachempati P, Krishnappa Salian KK, Singh V, Chhabra S, Shah S.(2015) Zirconia in dental implantology: A review. J Int Soc Prev Community Dent, 5(3): 147-156.
16. Osman R, Swain M. (2015) A Critical Review of Dental Implant Materials with an Emphasis on Titanium versus Zirconia. Materials, 8(3): 932-958.
17. Sailer I, Makarov NA, Thoma DS, Zwahlen M, Pjetursson BE. (2015) All-ceramic or metal-ceramic tooth-supported fixed dental prostheses (FDPs)? A systematic review of the survival and complication rates. Part I: Single crowns (SCs). Dent Mater, 31(6): 603-623.
18. Pjetursson BE, Sailer I, Makarov NA, Zwahlen M, Thoma DS. (2015) All-ceramic or metal-ceramic tooth-supported fixed dental prostheses (FDPs)? A systematic review of the survival and complication rates. Part II: Multiple-unit FDPs. Dent Mater, 31(6): 624-639.
19. Hashim D, Cionca N, Courvoisier DS, Mombelli A. (2016) A systematic review of the clinical survival of zirconia implants. Clin Oral Investig, 20(7): 1403-1417.
20. Sui X, Wei H, Wang D, Han Y, Deng J, Wang Y, Junjun W, Jianjun Y. (2014) Experimental research on the relationship between fit accuracy and fracture resistance of zirconia abutments. J Dent, 42(10): 1353-1359.

21. Wennerberg A, Albrektsson T. (2009) Effects of titanium surface topography on bone integration: a systematic review. Clin Oral Implants Res, 20(4): 172-184.
22. Elias CN, Lima JHC, Valiev R, Meyers MA. (2008) Biomedical applications of titanium and its alloys. J Miner met Mater Soc, 60(3): 46-49.
23. Barthes J, Ciftci S, Ponzio F, Knopf-Marques H, Pelyhe L, Gudima A, Kientzl I, Bognár E, Weszl M, Kzhyshkowska J, Vrana NE. Review: the potential impact of surface crystalline states of titanium for biomedical applications. (2018) Crit Rev Biotechnol, 38(3): 423-437.
24. Osborn JF. (1979) [Biomaterials and their application to implantation]. SSO Schweiz Monatsschr Zahnheilkd, 89(11): 1138-1139.
25. Cross MJ, Spycher J, Revell PA. Joint Replacement Technology.Woodhead Publishing, 2008: 190-211.
26. Pacifici L, De Angelis F, Orefici A, Cielo A. (2016) Metals used in maxillofacial surgery. Oral Implantol (Rome), 9 (Suppl 1/2016 to N 4/2016): 107-111.
27. Nallaswamy D. Textbook of Prosthodontics - eBook 2nd ed. Elsevier Health Sciences, 2017: 1263-1362
28. Chen Q, Thouas G. Biomaterials: A Basic Introduction. (Kinde Edition) CRC Press, 2015: 213-251
29. Londono R, Badylak SF. Host Response to Biomaterials. Academic Press, Oxford, 2015: 1-12.
30. Sáenz de Viteri V and Elena F. Tribology eBook - Fundamentals and Advancements, Chapter 5 - Titanium and Titanium Alloys as Biomaterials, 2013
31. Bajaj G, Bathiya A, Gade J, Mahale Y, Ulemale M, Atulkar M. Primary versus Secondary Implant Stability in Immediate and Early Loaded Implants. (2017) Int J Oral Health Med Res, 3(5): 49-54.
32. Smeets R, Stadlinger B, Schwarz F, Beck-Broichsitter B, Jung O, Precht C, Kloss F, Grübe A, Heiland M, Ebker T. (2016) Impact of Dental Implant Surface Modifications on Osseointegration. Biomed Res Int, 2016: 6285620
33. Mello ASdS, dos Santos PL, Marquesi A, Queiroz TP, Margonar R, de Souza Faloni AP. (2016) Some aspects of bone remodeling around dental implants. Rev Clin Periodontics Implantol Rehabil Oral, 11. 10.1016/j.piro.

34. Inoue M, Ono T, Kameo Y, Sasaki F, Ono T, Adachi T, Nakashima T. (2019) Forceful mastication activates osteocytes and builds a stout jawbone. Scientific Reports, 9(1): 4404.
35. Osstell. (2019) The Technique Behind Osstell - Implant Stability. Available from: https://www.osstell.com/clinical-guidelines/the-technique-behind-osstell/.
36. Gallucci GO, Benic GI, Eckert SE, Papaspyridakos P, Schimmel M, Schrott A, Weber HP. (2014) Consensus statements and clinical recommendations for implant loading protocols. Int J Oral Maxillofac Implants, 29: 287-290.
37. Patil R, Bharadwaj D. Is primary stability a predictable parameter for loading implant? (2016) J Int Clin Dent Res Organ. 8(1): 84-88.
38. Rodrigo D, Aracil L, Martin C, Sanz M. (2010) Diagnosis of implant stability and its impact on implant survival: a prospective case series study. Clin Oral Implants Res, 21(3): 255-261.
39. Cobo-Vázquez C, Reininger D, Molinero-Mourelle P, González-Serrano J, Guisado-Moya B, López-Quiles J. (2018) Effect of the lack of primary stability in the survival of dental implants. J Clin Exp Dent, 10(1): e14–e19.
40. Friberg B, Jisander S, Widmark G, Lundgren A, Ivanoff CJ, Sennerby L, Thorén C. (2003) One-year prospective three-center study comparing the outcome of a "soft bone implant" (prototype Mk IV) and the standard Branemark implant. Clin Implant Dent Relat Res, 5(2):71-77.
41. Chugh T, Jain AK, Jaiswal RK, Mehrotra P, Mehrotra R. (2013) Bone density and its importance in orthodontics. J Oral Biol Craniofac Res, 3(2): 92-97.
42. Misch CE. Contemporary Implant Dentistry. Elsevier, 1999: 137-146.
43. Pauwels R, Jacobs R, Singer SR, Mupparapu M. (2015) CBCT-based bone quality assessment: are Hounsfield units applicable? Dentomaxillofac Radiol, 44(1):20140238.
44. Elias CN, Rocha FA, Nascimento AL, Coelho PG. (2012) Influence of implant shape, surface morphology, surgical technique and bone quality on the primary stability of dental implants. J Mech Behav Biomed Mater, 16: 169-180.
45. Ryu HS, Namgung C, Lee JH, Lim YJ. (2014) The influence of thread geometry on implant osseointegration under immediate loading: a literature review. J Adv Prosthodont, 6(6): 547-554.

46. Herekar MG, Patil VN, Mulani SS, Sethi M, Padhye O. (2014) The influence of thread geometry on biomechanical load transfer to bone: A finite element analysis comparing two implant thread designs. Dent Res J (Isfahan), 11(4): 489-494.
47. Le Guehennec L, Soueidan A, Layrolle P, Amouriq Y. (2007) Surface treatments of titanium dental implants for rapid osseointegration. Dent Mater, 23(7): 844-854.
48. Noronha VT, Paula AJ, Duran G, Galembeck A, Cogo-Muller K, Franz-Montan M, Duran N. (2017) Silver nanoparticles in dentistry. Dent Mater, 33(10): 1110-1126.
49. Xuereb M, Camilleri J, Attard NJ. (2015) Systematic review of current dental implant coating materials and novel coating techniques. Int J Prosthodont, 28(1): 51-59.
50. The European Commission. Guidelines on medical devices - MEDDEV 2.7.1 (rev. 4) 2009.
51. Weszl M, Rencz F, Brodszky V. (2019) Is the trend of increasing use of patient-reported outcome measures in medical device studies the sign of shift towards value-based purchasing in Europe? Eur J Health Econ, 20(Suppl 1): 133-40.
52. Yeo IS. (2014) Reality of Dental Implant Surface Modification: A Short Literature Review. Open Biomed Eng J, 8: 114-119.
53. Almaguer-Flores A, Olivares-Navarrete R, Wieland M, Ximenez-Fyvie LA, Schwartz Z, Boyan BD. (2012) Influence of topography and hydrophilicity on initial oral biofilm formation on microstructured titanium surfaces in vitro. Clin Oral Implants Res, 23(3): 301-307.
54. Wennerberg A, Galli S, Albrektsson T. (2011) Current knowledge about the hydrophilic and nanostructured SLActive surface. Clin Cosmet Investig Dent. 3: 59–67.
55. Renvert S, Polyzois I, Claffey N. (2011) How do implant surface characteristics influence peri-implant disease? J Clin Periodontol, 38(11): 214-222.
56. Kolafova M, Stovicek J, Strnad J, Zemek J, Dybal J. (2017) In Vitro Bioactivity Test of Real Dental Implants According to ISO 23317. Int J Oral Maxillofac Implants, 32(6): 1221-1230.
57. Mamalis AA, Silvestros SS. (2011) Analysis of osteoblastic gene expression in the early human mesenchymal cell response to a chemically modified implant surface: an in vitro study. Clin Oral Implants Res, 22(5): 530-537.

58. Masaki C, Schneider GB, Zaharias R, Seabold D, Stanford C. (2005) Effects of implant surface microtopography on osteoblast gene expression. Clin Oral Implants Res, 16(6):650-656.
59. Zhao G, Schwartz Z, Wieland M, Rupp F, Geis-Gerstorfer J, Cochran DL, Boyan BD. (2005) High surface energy enhances cell response to titanium substrate microstructure. J Biomed Mater Res A, 74(1): 49-58.
60. Rausch-fan X, Qu Z, Wieland M, Matejka M, Schedle A. (2008) Differentiation and cytokine synthesis of human alveolar osteoblasts compared to osteoblast-like cells (MG63) in response to titanium surfaces. Dent Mater, 24(1): 102-110.
61. Zhao G, Raines AL, Wieland M, Schwartz Z, Boyan BD. (2007) Requirement for both micron- and submicron scale structure for synergistic responses of osteoblasts to substrate surface energy and topography. Biomaterials, 28(18): 2821-2829.
62. Wall I, Donos N, Carlqvist K, Jones F, Brett P. (2009) Modified titanium surfaces promote accelerated osteogenic differentiation of mesenchymal stromal cells in vitro. Bone, 45(1): 17-26.
63. Qu Z, Rausch-Fan X, Wieland M, Matejka M, Schedle A. (2007) The initial attachment and subsequent behavior regulation of osteoblasts by dental implant surface modification. J Biomed Mater Res A, 82(3): 658-668.
64. Bonfante EA, Janal MN, Granato R, Marin C, Suzuki M, Tovar N, Coelho PG. (2013) Buccal and lingual bone level alterations after immediate implantation of four implant surfaces: a study in dogs. Clin Oral Implants Res, 24(12): 1375-1380.
65. Bornstein MM, Hart CN, Halbritter SA, Morton D, Buser D. (2009) Early loading of nonsubmerged titanium implants with a chemically modified sand-blasted and acid-etched surface: 6-month results of a prospective case series study in the posterior mandible focusing on peri-implant crestal bone changes and implant stability quotient (ISQ) values. Clin Implant Dent Relat Res, 11(4): 338-347.
66. Duncan WJ, Lee MH, Dovban ASM, Hendra N, Ershadi S, Rumende H. (2008) Anodization increases early integration of osstem implants in sheep femurs. Ann R Australas Coll Dent Surg, 19: 152-156.
67. Burgess AV, Story BJ, Wagner WR, Trisi P, Pikos MA, Guttenberg SA. (1999) Highly crystalline MP-1 hydroxylapatite coating. Part II: In vivo performance on endosseous root implants in dogs. Clin Oral Implants Res, 10(4): 257-66.

68. Burgess AV, Story BJ, La D, Wagner WR, LeGeros JP. (1999) Highly crystalline MP-1 hydroxylapatite coating. Part I: In vitro characterization and comparison to other plasma-sprayed hydroxylapatite coatings. Clin Oral Implants Res, 10(4): 245-256.
69. Thierer T, Davliakos JP, Keith JD, Sanders JJ, Tarnow DP, Rivers JA. (2008) Five-Year Prospective Clinical Evaluation of Highly Crystalline HA MP-1–Coated Dental Implants. J Oral Implantol, 34(1): 39-46.
70. Citeau A, Guicheux J, Vinatier C, Layrolle P, Nguyen TP, Pilet P, Daculsi G. (2005) *In vitro* biological effects of titanium rough surface obtained by calcium phosphate grid blasting. Biomaterials, 26(2): 157-165.
71. Le Guehennec L, Lopez-Heredia MA, Enkel B, Weiss P, Amouriq Y, Layrolle P. (2008) Osteoblastic cell behaviour on different titanium implant surfaces. Acta Biomater, 4(3): 535-543.
72. Monjo M, Petzold C, Ramis JM, Lyngstadaas SP, Ellingsen JE. (2012) *In vitro* osteogenic properties of two dental implant surfaces. Int J Biomater, 2012:181024.
73. Bhatavadekar NB, Hu J, Keys K, Ofek G, Athanasiou KA. (2011) Novel application of cytodetachment technology to the analysis of dental implant surfaces. Int J Oral Maxillofac Implants, 26(5): 985-990.
74. Guo J, Padilla RJ, Ambrose W, De Kok IJ, Cooper LF. (2007)The effect of hydrofluoric acid treatment of TiO_2 grit blasted titanium implants on adherent osteoblast gene expression *in vitro* and i*n vivo*. Biomaterials, 28(36): 5418-5425.
75. Valencia S, Gretzer C, Cooper LF. (2009) Surface nanofeature effects on titanium-adherent human mesenchymal stem cells. Int J Oral Maxillofac Implants, 24(1): 38-46.
76. Rocci M, Rocci A, Martignoni M, Albrektsson T, Barlattani A, Gargari M. Comparing the TiOblast and Osseospeed surfaces. (2008) Histomorphometric and histological analysis in humans. Oral Implantol (Rome), 1(1): 34-42.
77. Das K, Bose S, Bandyopadhyay A. (2007) Surface modifications and cell-materials interactions with anodized Ti. Acta Biomater, 3(4): 573-585.
78. Kaluderovic MR, Schreckenbach JP, Graf HL. (2016) Titanium dental implant surfaces obtained by anodic spark deposition - From the past to the future. Mater Sci Eng C Mater Biol Appl, 69: 1429-1441.

79. Polizzi G, Gualini F, Friberg B. (2013) A two-center retrospective analysis of long-term clinical and radiologic data of TiUnite and turned implants placed in the same mouth. Int J Prosthodont, 26(4): 350-358.
80. Chrcanovic BR, Albrektsson T, Wennerberg A. (2016) Turned versus anodised dental implants: a meta-analysis. J Oral Rehabil, 43(9): 716-728.
81. Webster TJ, Ergun C, Doremus RH, Lanford WA. (2003) Increased osteoblast adhesion on titanium-coated hydroxylapatite that forms $CaTiO_3$. J Biomed Mater Res A, 67(3): 975-890.
82. Lee SY, Yang DJ, Yeo S, An HW, Ryoo KH, Park KB. (2012) The cytocompatibility and osseointegration of the Ti implants with XPEED® surfaces. Clinical Oral Implants Research, 23(11): 1283-1289.
83. Yoshinari M, Oda Y, Kato T, Okuda K, Hirayama A. (2000) Influence of surface modifications to titanium on oral bacterial adhesion in vitro. J Biomed Mater Res, 52(2): 388-394.
84. Gastaldi G, Grusovin MG, Felice P, Barausse C, Ippolito DR, Esposito M. (2017) Early loading of maxillary titanium implants with a nanostructured calcium-incorporated surface (Xpeed): 5-year results from a multicentre randomised controlled trial. Eur J Oral Implantol, 10(4): 415-424.
85. Coelho PG, Takayama T, Yoo D, Jimbo R, Karunagaran S, Tovar N, Janal MN, Yamano S. (2014) Nanometer-scale features on micrometer-scale surface texturing: a bone histological, gene expression, and nanomechanical study. Bone. 65: 25-32.
86. Coelho PG, Marin C, Granato R, Bonfante EA, Lima CP, Suzuki M. (2010) Surface treatment at the cervical region and its effect on bone maintenance after immediate implantation: an experimental study in dogs. Oral Surg Oral Med Oral Pathol Oral Radiol Endod, 110(2): 182-187.
87. Marin C, Granato R, Suzuki M, Gil JN, Piattelli A, Coelho PG. (2008) Removal torque and histomorphometric evaluation of bioceramic grit-blasted/acid-etched and dual acid-etched implant surfaces: an experimental study in dogs. J Periodontol, 79(10): 1942-1949.
88. Mendes VC, Moineddin R, Davies JE. (2007) The effect of discrete calcium phosphate nanocrystals on bone-bonding to titanium surfaces. Biomaterials, 28(32): 4748-4755.

89. Mendes VC, Moineddin R, Davies JE. (2009) Discrete calcium phosphate nanocrystalline deposition enhances osteoconduction on titanium-based implant surfaces. J Biomed Mater Res A, 90(2): 577-585.
90. Liu R, Lei T, Dusevich V, Yao X, Liu Y, Walker MP, Wang Y, Ye L. (2013) Surface characteristics and cell adhesion: a comparative study of four commercial dental implants. J Prosthodont, 22(8): 641-651.
91. Calvo-Guirado JL, Satorres-Nieto M, Aguilar-Salvatierra A, Delgado-Ruiz RA, Mate-Sanchez de Val JE, Gargallo-Albiol J, Gomez-Moreno G, Romanos GE. (2015) Influence of surface treatment on osseointegration of dental implants: histological, histomorphometric and radiological analysis *in vivo*. Clin Oral Investig, 19(2): 509-517.
92. Ostman PO, Wennerberg A, Ekestubbe A, Albrektsson T. (2013) Immediate occlusal loading of NanoTite tapered implants: a prospective 1-year clinical and radiographic study. Clin Implant Dent Relat Res, 15(6): 809-818.
93. Shin SY, Han DH. (2010) Influence of a microgrooved collar design on soft and hard tissue healing of immediate implantation in fresh extraction sites in dogs. Clin Oral Implants Res, 21(8): 804-814.
94. Alexander H, Ricci JL, Hrico GJ. (2009) Mechanical basis for bone retention around dental implants. J Biomed Mater Res B Appl Biomater, 88(2): 306-311.
95. Weiner S, Simon J, Ehrenberg DS, Zweig B, Ricci JL. (2008) The effects of laser microtextured collars upon crestal bone levels of dental implants. Implant Dent, 17(2): 217-228.
96. Nevins M, Nevins ML, Camelo M, Boyesen JL, Kim DM. (2008) Human histologic evidence of a connective tissue attachment to a dental implant. Int J Periodontics Restorative Dent, 28(2): 111-121.
97. Guarnieri R, Placella R, Testarelli L, Iorio-Siciliano V, Grande M. (2014) Clinical, radiographic, and esthetic evaluation of immediately loaded laser microtextured implants placed into fresh extraction sockets in the anterior maxilla: a 2-year retrospective multicentric study. Implant Dent, 23(2): 144-154.
98. Grande M, Ceccherini A, Serra M, Bava L, Farronato D, Iorio Siciliano V, Guarnieri R. (2013) Immediate occlusal loading of Tapered Internal Laser-Lok®

implants in partial arch rehabilitations: a 24-months clinical and radiographic study. J Osseointegration, 5(3): 53-60.

99. Pecora GE, Ceccarelli R, Bonelli M, Alexander H, Ricci JL. (2009) Clinical evaluation of laser microtexturing for soft tissue and bone attachment to dental implants. Implant Dent, 18(1): 57-66.
100. Botos S, Yousef H, Zweig B, Flinton R, Weiner S. (2011) The effects of laser microtexturing of the dental implant collar on crestal bone levels and peri-implant health. Int J Oral Maxillofac Implants, 26(3): 492-498.
101. Hindy A, Farahmand F, Tabatabaei FS. (2017) *In vitro* biological outcome of laser application for modification or processing of titanium dental implants. Lasers Med Sci, 32(5): 1197-1206.
102. Kurella A, Dahotre NB. (2005) Review paper: surface modification for bioimplants: the role of laser surface engineering. J Biomater Appl, 20(1): 5-50.
103. Frojd V, Chavez de Paz L, Andersson M, Wennerberg A, Davies JR, Svensater G. (2011) In situ analysis of multispecies biofilm formation on customized titanium surfaces. Mol Oral Microbiol, 26(4): 241-252.
104. Subramani K, Jung RE, Molenberg A, Hammerle CH. (2009) Biofilm on dental implants: a review of the literature. Int J Oral Maxillofac Implants, 24(4): 616-26.
105. L PC, Velitchka D-P, E. PV. (2019) Microbiology of Periodontal Diseases. A Review. Biotechnol Biotechnol Equip, 27(3): 3754-3759
106. Wassmann T, Kreis S, Behr M, Buergers R. (2017) The influence of surface texture and wettability on initial bacterial adhesion on titanium and zirconium oxide dental implants. Int J Implant Dent, 3(1): 32.
107. Scharf DR, Tarnow DP. (1993) Success rates of osseointegration for implants placed under sterile versus clean conditions. J Periodontol, 64(10): 954-956.
108. Pippi R. (2017) Post-Surgical Clinical Monitoring of Soft Tissue Wound Healing in Periodontal and Implant Surgery. Int J Med Sci, 14(8): 721-8.
109. Sculean A, Gruber R, Bosshardt DD. (2014) Soft tissue wound healing around teeth and dental implants. J Clin Periodontol, 41 Suppl 15:S6-22.
110. Politis C, Schoenaers J, Jacobs R, Agbaje JO. (2016) Wound Healing Problems in the Mouth. Front Physiol, 7: 507

111. Liddelow G, Klineberg I. (2011) Patient-related risk factors for implant therapy. A critique of pertinent literature. Aust Dent J, 56(4): 417-426.
112. Satyanarayana R, Sruthima G, Suresh SMC, Raju R, Bheemalingeshwar R, Meenakhsi I. (2015) Implant Failures—Diagnosis and Management. Int J Clin Impl Dent, 1(2): 51-59.
113. Annibali S, Ripari M, La Monaca G, Tonoli F, Cristalli M. (2008) Local complications in dental implant surgery: prevention and treatment. Oral Implantol (Rome), 1(1): 21-33.
114. Liu Y, Wang J. (2017) Influences of microgap and micromotion of implant-abutment interface on marginal bone loss around implant neck. Arch Oral Biol, 83: 153-160.
115. Robertson K, Shahbazian T, MacLeod S. (2015) Treatment of peri-implantitis and the failing implant. Dent Clin North Am, 59(2): 329-343.
116. Smeets R, Stadlinger B, Schwarz F, Beck-Broichsitter B, Jung O, Precht C, Kloss F, Gröbe A, Heiland M, Ebker T. (2016) Impact of Dental Implant Surface Modifications on Osseointegration. Biomed Res Int, 2016: 6285620.
117. Geraets W, Zhang L, Liu Y, Wismeijer D. (2014) Annual bone loss and success rates of dental implants based on radiographic measurements. Dentomaxillofac Radiol, 43(7): 20140007.
118. Ramanauskaite A, Juodzbalys G. (2016) Diagnostic Principles of Peri-Implantitis: a Systematic Review and Guidelines for Peri-Implantitis Diagnosis Proposal. J Oral Maxillofac Res, 7(3): e8.
119. Mombelli A, Muller N, Cionca N. (2012) The epidemiology of peri-implantitis. Clin Oral Implants Res, 23 Suppl 6:67-76.
120. Barbier L, Vander Sloten J, Krzesinski G, Schepers E, Van der Perre G. (1998) Finite element analysis of non-axial versus axial loading of oral implants in the mandible of the dog. J Oral Rehabil, 25(11): 847-858.
121. Linish V, Peteris A. (2003) Biological Response to Dental Implant Loading / Overloading. Implant Overloading: Empiricism or Science? Stomatologija, Baltic Dental and Maxillofacial Journal, 5:83-89.
122. Qian J, Wennerberg A, Albrektsson T. (2012) Reasons for marginal bone loss around oral implants. Clin Implant Dent Relat Res, 14(6): 792-807.

123. Correya BA, R Mahesh M, Joy PT, Jose I, Koli DK. (2017) FEM analysis of stress distribution around a dental implant and surrounding jaw bone. Glob J Res Anal, 6(11): 322-325
124. Dawood A, Marti Marti B, Tanner S. (2017) Peri-implantitis and the prosthodontist. Br Dent J, 223(5): 325-332.
125. Konstantinidis IK, Kotsakis GA, Gerdes S, Walter MH. (2015) Cross-sectional study on the prevalence and risk indicators of peri-implant diseases. Eur J Oral Implantol, 8(1): 75-88.
126. Dunning D, Meyerowitz JA, Holzberg AD. (1989) Ambiguity and self-evaluation: The role of idiosyncratic trait definitions in self-serving assessments of ability. J Pers Soc Psychol, 57(6): 1082-1090.
127. Romano PS, Mark DH. (1994) Bias in the Coding of Hospital Discharge Data and Its Implications for Quality Assessment. Med Care, 32(1): 81-90.
128. McGauran N, Wieseler B, Kreis J, Schüler YB, Kölsch H, Kaiser T. (2010) Reporting bias in medical research - a narrative review. Trials, 11:37.
129. Saini M, Singh Y, Arora P, Arora V, Jain K. (2015) Implant biomaterials: A comprehensive review. World J Clin Cases, 3(1):52-57.
130. Smeets R, Precht C, Hahn M, Jung O, Hartjen P, Heiland M, Gröbe A, Holthaus MG, Hanken H. (2017) Biocompatibility and Osseointegration of Titanium Implants with a Silver-Doped Polysiloxane Coating: An *In Vivo* Pig Model. Int J Oral Maxillofac Implants, 32(6): 1338-1345.
131. Slenters TV, Hauser-Gerspach I, Daniels AU, Fromm KM. (2008) Silver coordination compounds as light-stable, nano-structured and anti-bacterial coatings for dental implant and restorative materials. J Mater Chem, 18: 5359-5362
132. Hasan J, Crawford RJ, Ivanova EP. (2013) Antibacterial surfaces: the quest for a new generation of biomaterials. Trends Biotechnol, 31(5): 295-304.
133. Marassi V, Di Cristo L, Smith SGJ, Ortelli S, Blosi M, Costa AL, Reschiglian P, Volkov Y, Prina-Mello A. (2018) Silver nanoparticles as a medical device in healthcare settings: a five-step approach for candidate screening of coating agents. R Soc Open Sci, 5(1):171113.
134. Sodagar A, Akhoundi MSA, Bahador A, Jalali YF, Behzadi Z, Elhaminejad F, Mirhashemi AR. (2017) Effect of TiO_2 nanoparticles incorporation on antibacterial

properties and shear bond strength of dental composite used in Orthodontics. Dental Press J Orthod, 22(5):67-74.

135. Bienias J, Surowska B, Stoch A, Matraszek H, Walczak M. (2009) The influence of SiO_2 and SiO_2-TiO_2 intermediate coatings on bond strength of titanium and Ti6Al4V alloy to dental porcelain. Dent Mater, 25(9): 1128-1135.
136. Fathi HM, Johnson A. (2016) The effect of TiO_2 concentration on properties of apatite-mullite glass-ceramics for dental use. Dent Mater, 32(2): 311-322.
137. Presoto CD, Bortolatto JF, de Carvalho PP, Trevisan TC, Floros MC, Junior OB. (2016) New Parameter for In-Office Dental Bleaching. Case Rep Dent, 2016:6034757.
138. Sarina S, Waclawik ER, Zhu H. (2013) Photocatalysis on supported gold and silver nanoparticles under ultraviolet and visible light irradiation. Green Chem, 15: 1814-1833.
139. Hajipour MJ, Fromm KM, Ashkarran AA, Jimenez de Aberasturi D, de Larramendi IR, Rojo T, Serpooshan V, Parak WJ, Mahmoudi M. (2012) Antibacterial properties of nanoparticles. Trends Biotechnol, 30(10): 499-511.
140. Danilczuk M, Lund A, Sadlo J, Yamada H, Michalik J. (2006) Conduction electron spin resonance of small silver particles. Spectrochim Acta A Mol Biomol Spectrosc, 63(1): 189-191.
141. Prabhu S, Poulose EK. (2012) Silver nanoparticles: mechanism of antimicrobial action, synthesis, medical applications, and toxicity effects. International Nano Letters, 2(1): 32.
142. Agnihotri S, Mukherji S. (2013) Immobilized silver nanoparticles enhance contact killing and show highest efficacy: elucidation of the mechanism of bactericidal action of silver. Nanoscale, 5(16): 7328-7340.
143. Juan L, Zhimin Z, Anchun M, Lei L, Jingchao Z. (2010) Deposition of silver nanoparticles on titanium surface for antibacterial effect. Int J Nanomedicine, 5: 261-267.
144. Zhao L, Wang H, Huo K, Cui L, Zhang W, Ni H, Zhang Y, Wu Z, Chu PK. (2011) Antibacterial nano-structured titania coating incorporated with silver nanoparticles. Biomaterials, 32(24): 5706-5716.

145. Veres Á, Janovák L, Bujdosó T, Rica T, Fodor E, Tallósy S, Buzás N, Nagy E, Dékány I. (2012) Silver and Phosphate Functionalized Reactive TiO_2/Polymer Composite Films for Destructions of Resistent Bacteria Using Visible Light. J Adv Oxid Technol, 15(1): 205-216.
146. Ameen AP, Short RD, Johns R, Schwach G. (1993) The surface analysis of implant materials. 1. The surface composition of a titanium dental implant material. Clin Oral Implants Res, 4(3): 144-150.
147. Lausmaa J, Kasemo B, Mattsson H. (1990) Surface spectroscopic characterization of titanium implant materials. Appl Surf Sci, 44(2):133-146.
148. Sawase T, Hai K, Yoshida K, Baba K, Hatada R, Atsuta M. (1998) Spectroscopic studies of three osseointegrated implants. J Dent, 26(2): 119-124.
149. Kilpadi DV, Raikar GN, Liu J, Lemons JE, Vohra Y, Gregory JC. (1998) Effect of surface treatment on unalloyed titanium implants: spectroscopic analyses. J Biomed Mater Res, 40(4): 646-659.
150. NIST X-ray Photoelectron Spectroscopy Database. Available from: https://srdata.nist.gov/xps/
151. Gyorgyey A, Janovak L, Adam A, Kopniczky J, Toth KL, Deak A, Panayotov I, Cuisinier F, Dekany I, Turzo K. (2016) Investigation of the *in vitro* photocatalytic antibacterial activity of nanocrystalline TiO_2 and coupled TiO_2/Ag containing copolymer on the surface of medical grade titanium. J Biomater Appl, 31(1): 55-67.
152. Pelaez M, Nolan NT, Pillai SC, Seery MK, Falaras P, Kontos AG, Dunlop PSM, Hamilton JWJ, Byrne JA, O'Shea K, Entezari MH, Dionysiou DD. (2012) A review on the visible light active titanium dioxide photocatalysts for environmental applications. Appl Catal B, 125: 331-349.
153. Zhu S, Wang D. (2017) Photocatalysis: Basic Principles, Diverse Forms of Implementations and Emerging Scientific Opportunities. Adv Energy Mater, 7: 1700841.
154. Gunawan C, Teoh WY, Marquis CP, Lifia J, Amal R. (2009) Reversible antimicrobial photoswitching in nanosilver. Small, 5(3): 341-344.
155. Forster A, Ungvari K, Gyorgyey A, Kukovecz A, Turzo K, Nagy K. (2014) Human epithelial tissue culture study on restorative materials. J Dent, 42(1): 7-14.

156. Kitano Y, Okada N. (1983) Separation of the epidermal sheet by dispase. Br J Dermatol, 108(5): 555-560.
157. Billiau A, Edy V, Heremans H, Van Damme J, Desmyter J, Georgiades J, De Somer P. (1977) Human interferon: mass production in a newly established cell line, MG-63. Antimicrob Agents Chemother, 12(1): 11-15.
158. Mosmann T. (1983) Rapid colorimetric assay for cellular growth and survival: application to proliferation and cytotoxicity assays. J Immunol Methods, 65(1-2): 55-63.
159. Ungvari K, Pelsoczi IK, Kormos B, Oszko A, Rakonczay Z, Kemeny L, Radnai M, Nagy K, Fazekas A, Turzó K. (2010) Effects on titanium implant surfaces of chemical agents used for the treatment of peri-implantitis. J Biomed Mater Res B Appl Biomater, 94(1): 222-229.
160. Bio-Rad (2018) alamarBlue® Technical Datasheet IFU. Available from: https://www.bio-rad-antibodies.com/static/uploads/ifu/buf012a.pdf
161. Veres Á, Ménesi J, Juhász Á, Berkesi O, Ábrahám N, Bohus G,Oszkó A, Pótári G, Buzás N, Janovák L, Dékány I. (2014) Photocatalytic performance of silver-modified TiO_2 embedded in poly (ethyl-acrylate-co-methyl metacrylate) matrix. Colloid Polym Sci, 292(1): 207-217.
162. Györgyey A, Csapó E, Ménesi J, Veres Á, Urbán E, Gergely C, Buzás K, Rakonczay Z, Nagy K, Cuisinier F, Dékány I, Turzó K. (2012) TiO_2-Ag/Au/polymer nanohybrid coatings targeting prevention of peri-implant infections of dental implants. SIWAN5 5th Szeged International Workshop on Advances in Nanoscience; Szeged, Hungary.
163. Foundation PS. Python Language Reference. Version 2.7.8 ed2015.
164. R Development C. TEAM 2011: R: A Language and Environment for Statistical Computing. R Foundation for Statistical Computing, Vienna, 2013(version 3.2.1.).
165. Sartoretto SC, Alves A, Resende RFB, Calasans-Maia J, Granjeiro JM, Calasans-Maia MD. (2015) Early osseointegration driven by the surface chemistry and wettability of dental implants. J Appl Oral Sci, 23(3): 279-287
166. Abraham CM. (2014) A Brief Historical Perspective on Dental Implants, Their Surface Coatings and Treatments. Open Dent J. 8: 50–55.

167. Palmquist A, Engquist H, Lausmaa J, Thomsen P. (2012) Commercially Available Dental Implants: Review of Their Surface Characteristics. J Biomater Tissue Eng, 2(2): 112-124.
168. Wennerberg A, Albrektsson T . (2006) Implant surfaces beyond micron roughness: Experimental and clinical knowledge of surface topography and surface chemistry. Inter Dent SA, 8(8): 14-18.
169. Lin HY, Liu Y, Wismeijer D, Crielaard W, Deng DM. (2013) Effects of oral implant surface roughness on bacterial biofilm formation and treatment efficacy. Int J Oral Maxillofac Implants, 28(5):1226-1231.
170. Schmidlin PR, Müller P, Attin T, Wieland M, Hofer D, Guggenheim B. (2013) Polyspecies biofilm formation on implant surfaces with different surface characteristics. J Appl Oral Sci, 21: 48-55.
171. Teughels W, Van Assche N, Sliepen I, Quirynen M. (2006) Effect of material characteristics and/or surface topography on biofilm development. Clin Oral Implants Res, 17 Suppl 2: 68-81.
172. Gristina GA. (1987) Biomaterial-centered infection: microbial adhesion versus tissue integration. Science, 237(4822):1588-1595.
173. Busscher HJ, van der Mei HC, Subbiahdoss G, Jutte PC, van den Dungen JJ, Zaat SA, Schultz MJ, Grainger DW. (2012) Biomaterial-associated infection: locating the finish line in the race for the surface. Sci Transl Med, 4(153): 153rv10.
174. Bai Y, Mora-Sero I, De Angelis F, Bisquert J, Wang P. (2014) Titanium dioxide nanomaterials for photovoltaic applications. Chem Rev, 114(19): 10095-10130.
175. Tilmaciu CM, Mathieu M, Lavigne JP, Toupet K, Guerrero G, Ponche A, Amalric J, Noel D, Mutin PH. (2015) *In vitro* and *in vivo* characterization of antibacterial activity and biocompatibility: a study on silver-containing phosphonate monolayers on titanium. Acta Biomater, 15: 266-277.
176. Massa MA, Covarrubias C, Bittner M, Fuentevilla IA, Capetillo P, Von Marttens A, Carvajal JC. (2014) Synthesis of new antibacterial composite coating for titanium based on highly ordered nanoporous silica and silver nanoparticles. Mater Sci Eng C Mater Biol Appl, 45: 146-153.

177. Arteagoitia I, Rodríguez-Andrés C, Rodríguez-Sánchez F. (2018) Antibiotic prophylaxis habits in dental implant surgery among dentists in Spain. A cross-sectional survey. Med Oral Patol Oral Cir Bucal, 23(5): 608-618.
178. Lund B, Hultin M, Tranaeus S, Naimi-Akbar A, Klinge B. (2015) Complex systematic review - Perioperative antibiotics in conjunction with dental implant placement. Clin Oral Implants Res, 26 Suppl 11: 1-14.
179. Lang NP, Berglundh T, Heitz-Mayfield LJ, Pjetursson BE, Salvi GE, Sanz M. (2004) Consensus statements and recommended clinical procedures regarding implant survival and complications. Int J Oral Maxillofac Implants, 19 Suppl:150-154.
180. Kędziora A, Speruda M, Krzyżewska E, Rybka J, Łukowiak A, Bugla-Płoskońska G. (2018) Similarities and Differences between Silver Ions and Silver in Nanoforms as Antibacterial Agents. Int J Mol Sci, 19(2): 444
181. Dakal TC, Kumar A, Majumdar RS, Yadav V. (2016) Mechanistic Basis of Antimicrobial Actions of Silver Nanoparticles. Front Microbiol, 7: 1831
182. Masa R, Deak A, Braunitzer G, Toth Z, Kopniczky J, Pelsoczi-Kovacs I, Ungvári K, Dékány I, Turzó K, . (2018) TiO(2)/Ag-TiO(2) Nanohybrid Films are Cytocompatible with Primary Epithelial Cells of Human Origin: An *In Vitro* Study. J Nanosci Nanotechnol, 18(6): 3916-3924.
183. Cao X, Tang M, Liu F, Nie Y, Zhao C. (2010) Immobilization of silver nanoparticles onto sulfonated polyethersulfone membranes as antibacterial materials. Colloids Surf B Biointerfaces, 81(2): 555-562.

10 PUBLICATION LIST

Publications related to the present thesis

1. **Györgyey Á**, Janovák L, Ádám A, Kopniczky J, Tóth KL, Deák Á, Panayotov I, Nagy K, Cuisinier F, Dékány I, Turzó K. (2016) Investigation of the *in vitro* photocatalytic antibacterial activity of nano-crystalline TiO_2 and coupled TiO_2/Ag containing copolymer on the surface of medical grade titanium.
   J Biomater Appl, 31(1): 55-67.

   IF: 2,31

2. Forster A, Ungvári K, **Györgyey Á**, Kukovecz Á, Turzó K, Nagy K. (2014) Human epithelial tissue culture study on restorative materials.
   J Dent, 42(1): 7-14.

   IF: 2,749

3. **Györgyey Á**, Ungvári K, Kecskeméti G, Kopniczky J, Hopp B, Oszkó A, Pelsőczi I, Rakonczay Z, Nagy K, Turzó K. (2013) Attachment and proliferation of human osteoblast-like cells (MG-63) on laser-ablated titanium implant material.
   J Mat Sci Eng C, 33(7): 4251-4259.

   IF: 2,736

11 ACKNOWLEDGMENTS

I would like to express my sincere gratitude to Dr. Zsombor Lacza, my supervisor. I would like to thank Professor Zoltán Benyó for providing me a supportive environment in the Institute of Clinical Experimental Research to finish my doctoral thesis. I would also like to thank Professor László Rosivall for providing me the opportunity to join the Doctoral School of Basic and Translational Medicine. I would like to thank Krisztina Buzás and the members in the Laboratory of Tumor Immunology and Pharmacology (Biological Research Center, Hungarian Academy of Sciences) for introducing me in the science of microbiology and for providing me a friendly and supportive work atmosphere. I would like to thank Frédéric Cuisinier and the members of the Laboratory of Bioengineering and Nanoscience (University of Montpellier I) for showing me the passion of dental research and cell culture. I would like to thank Professor Béla Hopp for his support. I also would like to thank to all contributors, co-authors, my colleagues, my friends, and my family for their help throughout my studies. I especially thank to Miklós Weszl for our discussions, his support and encouragement throughout the years.